The Astrophysical Journal, 715:277–291, 2010 May 20 doi:10.1088/0004-637X/715/1/277

INSIGHTS INTO THE CEPHEID DISTANCE SCALE

G. Bono[1,2], F. Caputo[2], M. Marconi[3], and I. Musella[3]
[1] Dipartimento di Fisica, Università di Roma Tor Vergata, Via della Ricerca Scientifica 1, 00133 Rome, Italy; bono@roma2.infn.it
[2] INAF–Osservatorio Astronomico di Roma, Via Frascati 33, 00040 Monte Porzio Catone, Italy; caputo@oa-roma.inaf.it
[3] INAF–Osservatorio Astronomico di Capodimonte, Via Moiariello 16, 80131 Napoli, Italy; marcella.marconi@oacn.inaf.it, ilaria.musella@oacn.inaf.it
Received 2010 February 24; accepted 2010 April 1; published 2010 April 27

ABSTRACT

We present a detailed investigation of the Cepheid distance scale by using both theory and observations. Through the use of pulsation models for fundamental mode Cepheids, we found that the slope of the period–luminosity (*P–L*) relation covering the entire period range ($0.40 \leqslant \log P \leqslant 2.0$) becomes steeper when moving from optical to near-infrared (NIR) bands, and that the metallicity dependence of the slope decreases from the *B*- to the *K* band. The sign of the metallicity dependence for the slopes of the $P–L_V$ and $P–L_I$ relation is at odds with some recent empirical estimates. We determined new homogeneous estimates of *V*- and *I*-band slopes for 87 independent Cepheid data sets belonging to 48 external galaxies with nebular oxygen abundance $7.5 \leqslant 12 + \log(\mathrm{O/H}) \leqslant 8.9$. By using Cepheid samples including more than 20 Cepheids, the χ^2 test indicates that the hypothesis of a steepening of the $P–L_{V,I}$ relations with increased metal content can be discarded at the 99% level. On the contrary, the observed slopes agree with the metallicity trend predicted by pulsation models, i.e., the slope is roughly constant for galaxies with $12+\log(\mathrm{O/H}) < 8.17$ and becomes shallower in the metal-rich regime, with confidence levels of 62% and 92%, respectively. The χ^2 test concerning the hypothesis that the slope does not depend on metallicity gives confidence levels either similar (PL_V, 62%) or smaller (PL_I, 67%). We investigated the dependence of the period–Wesenheit (*P–W*) relations on the metal content and we found that the slopes of optical and NIR *P–W* relations in external galaxies are similar to the slopes of Large Magellanic Cloud (LMC) Cepheids. They also agree with the theoretical predictions suggesting that the slopes of the *P–W* relations are independent of the metal content. On this ground, the *P–W* relations provide a robust method to determine distance moduli relative to the LMC, but theory and observations indicate that the metallicity dependence of the zero point in the different passbands has to be taken into account. To constrain this effect, we compared the independent set of galaxy distances provided by Rizzi et al. using the tip of the red giant branch with our homogeneous set of extragalactic Cepheid distances based on the *P–W* relations. We found that the metallicity correction on distances based on the *P–WBV* relation is $\gamma_{B,V} = -0.52$ mag dex^{-1}, whereas it is vanishing for the distances based on the *P–WVI* and on the *P–WJK* relations. These findings fully support Cepheid theoretical predictions.

Key words: Galaxy: disk – Local Group – Magellanic Clouds – stars: distances – stars: oscillations – stars: variables: Cepheids

Online-only material: machine-readable tables

1. INTRODUCTION

The cosmic distance scale and the estimate of the Hubble constant, H_0, are tightly connected with the period–luminosity (*P–L*) relation of Classical Cepheids and the distances to external galaxies are traditionally determined by using a universal *P–L* linear relation based on the Large Magellanic Cloud (LMC) variables.

However, theoretical predictions based on nonlinear, convective Cepheid models computed by our group (see Caputo 2008 for a comprehensive list of references) indicate that the instability strip boundaries in the $\log L$–$\log T_e$ plane are almost linear, but when transformed into the different period–magnitude planes they are better described by quadratic *P–L* relations. In particular, we found that at fixed metal content: (1) the predicted optical *P–L* relations can be properly fit with quadratic relations, (2) a discontinuity around $\log P \sim 1.2$ should be adopted to constrain the theoretical results into linear approximations, and (3) the predicted *P–L* relations become more and more linear and tight when moving from optical to near-infrared bands. Moreover, we suggested that the metal-poor Cepheids follow *P–L* relations which are steeper and brighter than the metal-rich ones, with the amount of this metallicity effect again decreasing from the *B*- to the *K* band. Furthermore, we drew attention to the evidence that the metallicity effect on the predicted period–Wesenheit (*P–W*) relations, which present several advantages when compared with the *P–L* relations, significantly depends on the adopted Wesenheit function.

With a few exceptions, these theoretical results have been considered with a certain skepticism. Only during the last few years, several observational investigations disclosed the nonlinearity of the *P–L* relation (Tammann et al. 2003; Ngeow et al. 2005; Ngeow & Kanbur 2006), as well as the evidence that the Cepheid *P–L* relation cannot be universal and that both the slope and the zero point might change from galaxy to galaxy. Quoting Sandage et al. (2009), "the existence of a universal *P–L* relation is an only historically justified illusion."

According to this new empirical evidence, which might imply severe limits in the precision of Cepheid distances, we examine the available observations by using the theoretical framework provided by the pulsation models and we address three main issues concerning the Cepheid distance scale: the intrinsic features of the *P–L* and the *P–W* relations, the dependence of the *P–L* and *P–W* slopes on the Cepheid metal content, and the impact of the metallicity effect on the Cepheid distances.

Table 1
Parameters of the Computed Pulsation Models

Z	Y	ΔM	L	l/H_p
0.004	0.25	3.5–11.0	L_{can}, L_{over}	1.5–1.8
0.008	0.25	3.5–11.0	L_{can}, L_{over}	1.5–1.8
0.01	0.26	5.0–11.0	L_{can}	1.5–1.8
0.02	0.25;0.26;0.28;0.31	5.0–11.0	L_{can}, L_{over}	1.5–1.8
0.03	0.275;0.31;0.335	5.0–11.0	L_{can}	1.5
0.04	0.25;0.29;0.33	5.0–11.0	L_{can}	1.5

Notes. From left to right: heavy element abundance (Z), helium content (Y), range in mass (ΔM, in solar units), luminosity (L), and mixing-length parameter (l/H_p). The adopted luminosity refers to the canonical mass–luminosity relation (L_{can}) or to higher levels (L_{over}) predicted by evolutionary models accounting for mild convective core overshooting and/or affected by mass loss before or during the Cepheid phase (see the text for details).

2. INTRINSIC FEATURES OF THE *P–L* RELATION

2.1. Predictions Based on Pulsation Models

The theoretical framework we developed during the last 10 years was already described in a series of papers (see, e.g., Bono et al. 1999a; Caputo 2008; Marconi 2009) and its main lines can be summarized as follows.

1. A nonlinear, nonlocal, and time-dependent convective code is used to calculate several model sequences (see Table 1) with constant chemical composition, mass, and luminosity, by varying the effective temperature T_e with steps of 100 K in order to properly cover the pulsation region. For metal abundances $Z \geqslant 0.02$, the adopted helium content Y accounts for different values of the helium-to-metals enrichment ratio $\Delta Y/\Delta Z$. For each chemical composition and mass value, the luminosity is fixed using a mass–luminosity (ML) relation based on evolutionary models that either neglect ("canonical") or account for convective core overshooting during central hydrogen burning phases ("overshooting"). the canonical ML relation adopted to construct our pulsation models is that given by Bono et al. (2000):

$$\log L_{can} = 0.90 + 3.35 \log M + 1.36 \log Y - 0.34 \log Z, \quad (1)$$

which has a standard deviation $\sigma = 0.02$ and accounts for both the blueward and the redward crossing of the instability strip. Note that, together with minor discrepancies among the canonical ML relations provided by different authors (see also Girardi et al. 2000; Castellani et al. 2003; Bertelli et al. 2009; Valle et al. 2009, and references therein), a variation in luminosity with respect to the canonical level can be due either to convective core overshooting or to mass loss before or during the He-burning phases. In the former case, stellar structures at fixed mass and chemical composition are over-luminous by $\log L/L_{can} = 0.25$ (see Chiosi et al. 1993), while in the latter the stellar structures at fixed luminosity and chemical composition are less massive (see Castellani & Degl'Innocenti 1995; Bono et al. 2000; Castellani et al. 2003). The net consequence of the quoted physical mechanisms is a positive $\log L/L_{can}$ ratio. Finally, all the pulsation models are calculated assuming a mixing-length parameter[4] $l/H_p = 1.5$, but several additional models were computed by adopting $l/H_p = 1.7$ and 1.8.

2. The adopted approach provides not only the pulsation equation $P = f(Z, Y, M, L, T_e)$ and the blue (hot) boundaries of the instability strip, but also robust predictions concerning the red (cool) boundaries together with the pulsation amplitudes (i.e., light and radial velocity curves).
3. Once the edges of the pulsation region in the H-R diagram are determined, the instability strip is populated according to a period–mass distribution $P(M) \sim 1/M^3$ suggested by Kennicutt et al. (1998) and two different procedures for the Cepheid luminosity. For each mass and chemical composition, we adopted (a) the canonical luminosity given by Equation (1) (Caputo et al. 2000), and (b) the evolutionary tracks computed by Pietrinferni et al. (2004) with a Reimers mass-loss parameter $\eta = 0.4$ (see Fiorentino et al. 2007, for more details). In the latter case, we also take into account the evolutionary time spent by the Cepheids inside the strip.
4. For each predicted pulsator, we calculate the period by means of the pulsation equation and the absolute magnitude in the various photometric bands by using the model atmospheres by Castelli et al. (1997a, 1997b). Eventually, we derive with a standard regression the multiband *P–L* relations. Note that these synthetic *P–L* relations refer to *static* magnitudes, i.e., the magnitude the star would have, if it were not pulsating (Bono et al. 1999b).

As a whole, the synthetic *P–L* relations depend on the adopted ML relation, on the procedure adopted to populate the instability strip, on the helium content Y (at fixed l/H_p and Z, see Fiorentino et al. 2002; Marconi et al. 2005) and on the mixing-length parameter l/H_p (at fixed Z and Y, see Fiorentino et al. 2007). However, the quoted parameters and assumptions mainly affect the zero point of the *P–L* relations, but the slope shows minimal changes. According to the above evidence, we used all the synthetic populations of fundamental models to derive the average *P–L* slope for the different bands listed in Table 2 as a function of the chemical composition parameter $\log(Z/X)$, where X is the hydrogen content ($X = 1 - Z - Y$). We fit the predicted fundamental pulsators with $0.4 \leqslant \log P \leqslant 2.0$ with a linear regression $M_i = a + b \log P$ to determine the slope b_{all}. Then, the pulsators with $\log P \leqslant 1$ and $\log P > 1$ were used to derive b_{short} and b_{long}, respectively. The predicted dependence of the overall slopes on the chemical composition $\partial b_{all}/\partial \log(Z/X)$, in the quoted metallicity range, are also listed in Table 2. Note that no synthetic *P–L* relations are presently available for $Z < 0.004$ but we show in Figure 1 that pulsation models recently computed with $Z = 0.001$ and $Y = 0.24$ (M. Marconi et al. 2010, in preparation) appear in close agreement with the period–magnitude location of more metal-rich pulsators ($Z = 0.004$). This finding seems to suggest that the slope of the *P–L* relation is marginally affected by the metal abundance for chemical compositions more metal-poor than $\log(Z/X) = -2.27$.

In order to make the following comparison between theory and observations easier, we give in Table 3 the oxygen and iron abundances of the pulsation models which were derived by adopting scaled-solar chemical compositions and the solar chemical composition ($\log(Z/X)_\odot = -1.78$, $12+\log(O/H)_\odot = 8.66$) from Asplund et al. (2004).

The slopes of the predicted *P–L* relations plotted in Figure 2 (see also Table 2) as a function of $\log(Z/X)$ show that they become steeper by increasing the filter wavelength, in agreement with well-known empirical results (see, e.g., Madore & Freedman 1991). An increase in the metal content causes a

[4] The mixing-length parameter is a measure of the convection efficiency. It is used to close the system of equations describing the dynamical and convective stellar structure.

Table 2
Predicted Slopes (b) of Synthetic Linear P–L Relations $M_i = a + b \log P$ for the Chemical Compositions Listed in Table 1

Band	$\log(Z/X)$	$b_{\rm all}$	$b_{\rm short}$	$b_{\rm long}$
M_B	−2.27	-2.68 ± 0.13	-3.04 ± 0.16	-2.00 ± 0.15
M_B	−1.97	-2.51 ± 0.16	-2.89 ± 0.12	-1.92 ± 0.15
M_B	−1.86	-2.33 ± 0.16	-2.86 ± 0.12	-1.62 ± 0.15
M_B	−1.55	-2.10 ± 0.28	-2.23 ± 0.21	-1.66 ± 0.13
M_B	−1.34	-1.77 ± 0.17	-1.81 ± 0.19	-1.74 ± 0.13
M_B	−1.22	-1.77 ± 0.17	-1.91 ± 0.22	-1.82 ± 0.15
		$\partial b_{\rm all}(M_B)/\partial \log(Z/X) = 0.94 \pm 0.07$		
M_V	−2.27	-2.87 ± 0.09	-3.22 ± 0.08	-2.44 ± 0.14
M_V	−1.97	-2.80 ± 0.15	-2.97 ± 0.10	-2.39 ± 0.14
M_V	−1.86	-2.69 ± 0.10	-3.19 ± 0.10	-2.14 ± 0.14
M_V	−1.55	-2.51 ± 0.24	-2.60 ± 0.18	-2.28 ± 0.12
M_V	−1.34	-2.21 ± 0.13	-2.33 ± 0.15	-2.23 ± 0.10
M_V	−1.22	-2.25 ± 0.17	-2.51 ± 0.22	-2.31 ± 0.18
		$\partial b_{\rm all}(M_V)/\partial \log(Z/X) = 0.67 \pm 0.09$		
M_I	−2.27	-3.00 ± 0.07	-3.28 ± 0.04	-2.76 ± 0.10
M_I	−1.97	-2.90 ± 0.13	-3.12 ± 0.06	-2.70 ± 0.10
M_I	−1.86	-2.91 ± 0.06	-3.30 ± 0.09	-2.55 ± 0.10
M_I	−1.55	-2.80 ± 0.19	-2.88 ± 0.13	-2.61 ± 0.10
M_I	−1.34	-2.56 ± 0.09	-2.68 ± 0.12	-2.61 ± 0.05
M_I	−1.22	-2.61 ± 0.13	-2.69 ± 0.12	-2.63 ± 0.15
		$\partial b_{\rm all}(M_I)/\partial \log(Z/X) = 0.45 \pm 0.08$		
M_J	−2.27	-3.16 ± 0.06	-3.33 ± 0.05	-2.81 ± 0.10
M_J	−1.97	-3.13 ± 0.11	-3.30 ± 0.04	-2.77 ± 0.10
M_J	−1.86	-3.10 ± 0.06	-3.37 ± 0.10	-2.73 ± 0.10
M_J	−1.55	-3.00 ± 0.11	-3.06 ± 0.16	-2.81 ± 0.09
M_J	−1.34	-2.90 ± 0.09	-2.94 ± 0.10	-2.80 ± 0.05
M_J	−1.22	-2.92 ± 0.11	-2.95 ± 0.08	-2.83 ± 0.15
		$\partial b_{\rm all}(M_J)/\partial \log(Z/X) = 0.27 \pm 0.03$		
M_K	−2.27	-3.19 ± 0.09	-3.33 ± 0.04	-3.04 ± 0.09
M_K	−1.97	-3.28 ± 0.09	-3.34 ± 0.04	-3.02 ± 0.09
M_K	−1.86	-3.31 ± 0.03	-3.47 ± 0.06	-3.05 ± 0.09
M_K	−1.55	-3.22 ± 0.15	-3.28 ± 0.10	-3.08 ± 0.08
M_K	−1.34	-3.16 ± 0.06	-3.18 ± 0.08	-3.13 ± 0.05
M_K	−1.22	-3.16 ± 0.09	-3.17 ± 0.08	-3.12 ± 0.13
		$\partial b_{\rm all}(M_K)/\partial \log(Z/X) = 0.08 \pm 0.07$		

Notes. The subscript *all* refers to all the fundamental pulsators with $0.4 \leqslant \log P \leqslant 2.0$, while *short* and *long* refer to those with $\log P \leqslant 1.0$, and with $\log P > 1.0$, respectively. For each band, the dependence $\partial b_{\rm all}/\partial \log(Z/X)$ is also listed. Note that for $Z \geqslant 0.02$, the labeled ratio Z/X is the mean value of the various helium abundances listed in Table 1.

Table 3
Oxygen and Iron Abundances of the Computed Pulsation Models, as Derived for Scaled-solar Chemical Compositions and by Adopting the Solar Abundances from Asplund et al. (2004)

Z	Y	$\log(Z/X)$	12+log(O/H)	[Fe/H]
0.001	0.24	−2.87	7.56	−1.10
0.004	0.25	−2.27	8.17	−0.49
0.008	0.25	−1.97	8.47	−0.18
0.01	0.26	−1.86	8.58	−0.08
0.02	0.25	−1.56	8.88	+0.22
0.02	0.26	−1.56	8.89	+0.23
0.02	0.28	−1.54	8.90	+0.24
0.02	0.31	−1.53	8.92	+0.26
0.03	0.275	−1.36	9.08	+0.42
0.03	0.31	−1.34	9.10	+0.44
0.03	0.335	−1.33	9.12	+0.46
0.04	0.25	−1.25	9.19	+0.53
0.04	0.29	−1.22	9.22	+0.56
0.04	0.33	−1.20	9.25	+0.59

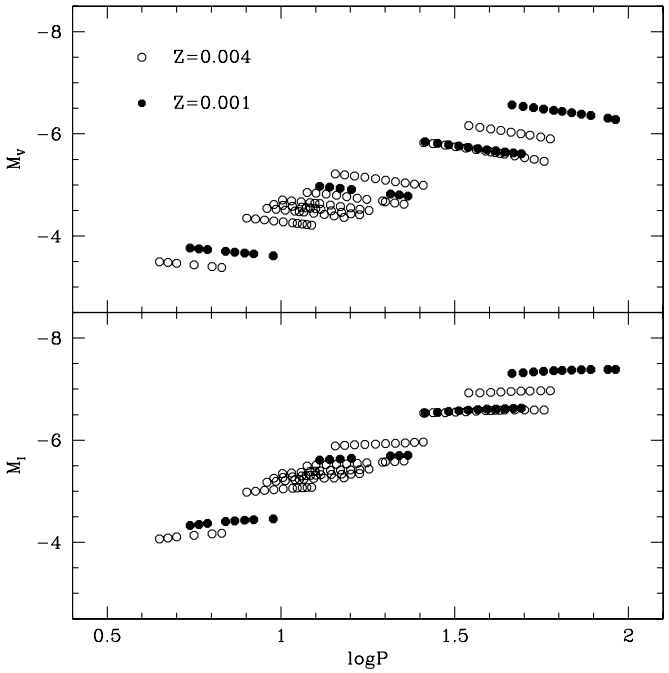

Figure 1. Comparison between pulsation models with different metal contents, namely $Z = 0.001$ (solid circles) and $Z = 0.004$ (open circles).

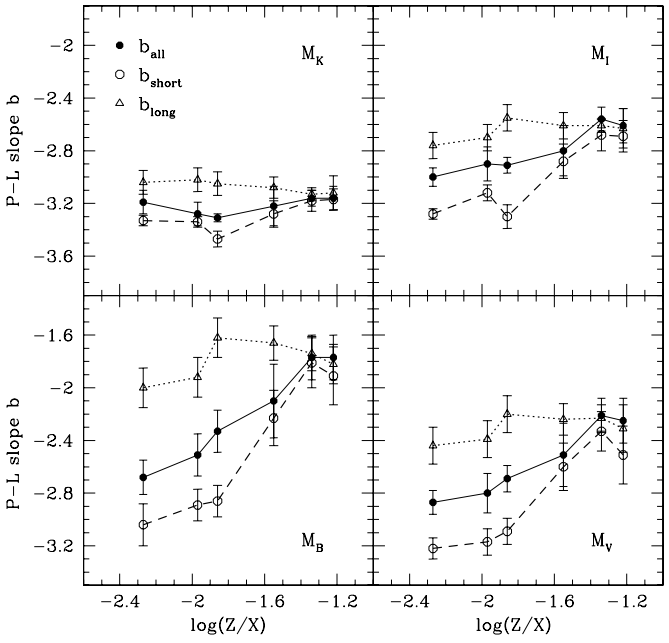

Figure 2. Predicted slopes (b) of linear P–L relations based on pulsation models with metal content ranging from $Z = 0.004$ to $Z = -0.04$. The standard regression including all the predicted pulsators gives the slopes $b_{\rm all}$ (solid line), while the slopes $b_{\rm short}$ (dashed line) and $b_{\rm long}$ (dotted line) were evaluated using short- ($\log P \leqslant 1$) and long-period ($\log P > 1$) pulsators, respectively.

flattening in the optical (BVI) P–L relations, while the slopes of the short-period relations (dashed lines) are typically steeper than those for long-period ones (dotted lines). Again, the amplitude of these two effects decreases as the filter wavelength increases. In the NIR JK bands, the dependence of the slope, both on the period range and on the metal content, is significantly reduced.

For a first comparison with observations, we list in Table 4 the slopes for the P–L relations of fundamental Cepheids available

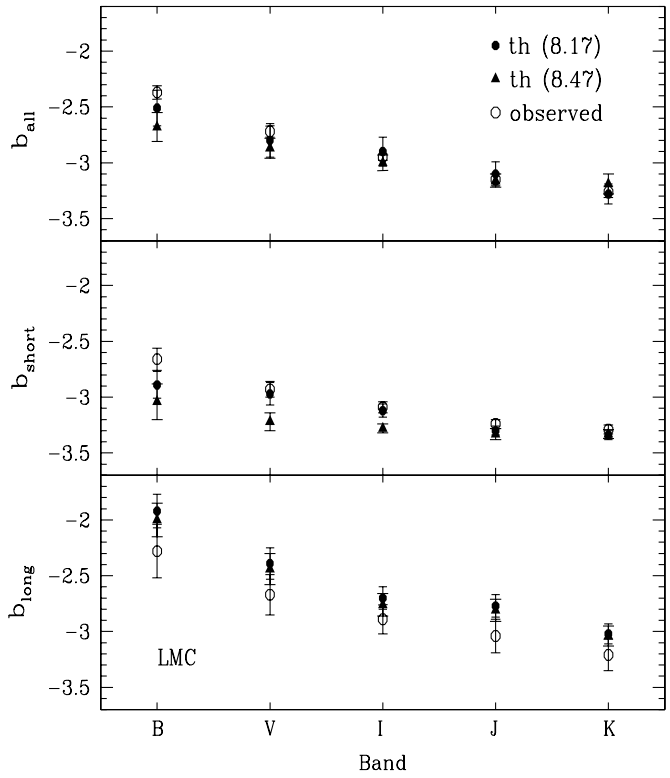

Figure 3. Comparison between observed slopes of LMC *P–L* relations (open circles) with the predicted values for a chemical composition of 12+log(O/H) = 8.17 (filled circles) and of 8.47 (filled triangles).

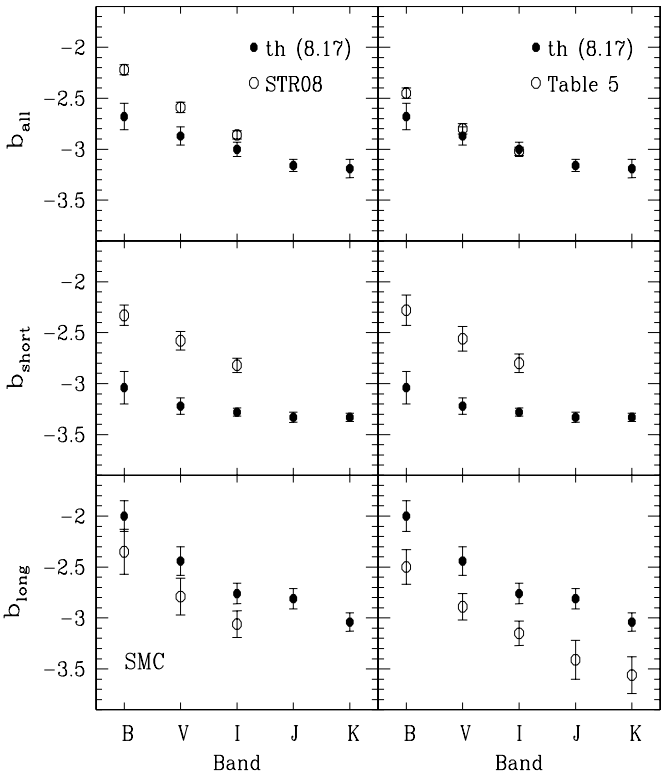

Figure 4. Comparison between predicted slopes for a metal content of $Z = 0.004$ (filled circles) and observed values of the SMC *P–L* relations (open circles), using the results by STR08 (left panel) and the ones from our Table 5 (right panel).

in the most recent literature for the Magellanic Clouds, the Milky Way (MW), and M31.

2.2. Magellanic Clouds

The investigations focused on LMC Cepheids, the most accurate sample, disclose the expected steepening of the *P–L* relations, when moving from optical to NIR magnitudes. Moreover, they show that the optical *P–L* relations of short ($\log P \leqslant 1$) and long-period ($\log P > 1$) Cepheids do have statistically different slopes with the evidence of a flattening in the long period regime. On the other hand, the slopes of the *P–L*$_K$ relation do not show any significant difference (see the discussions in Sandage et al. 2004, hereinafter STR04; and Ngeow et al. 2008, hereinafter NKN08). The quoted trends agree quite well with current predictions, and indeed data plotted in Figure 3 show that the observed slopes attain *values* similar to the predicted ones for a chemical composition of 12+log(O/H) = 8.17 and of 8.47 dex.

The analysis by STR08 of the SMC variables relies on OGLE *BVI* data. This sample includes 344 Cepheids with periods ranging from $\log P \sim 0.50$ to $\log P \sim 1.62$ and seems to suggest a steepening in the long-period range, although the difference in the slope between short- and long-period Cepheids is within $\sim 1\sigma$ and less significant than for LMC Cepheids. In order to extend the analysis of SMC Cepheids to periods longer than the OGLE Cepheids and to near-infrared bands, we have used additional *BVI* data (75 Cepheids, $0.93 \leqslant \log P \leqslant 1.93$) from Caldwell & Coulson (1984) and *JK* data (22 Cepheids, $0.93 \leqslant \log P \leqslant 1.93$) from Laney & Stobie (1986). Then, we fit with a standard regression all the variables with $\log P \geqslant 0.5$, as well as to the subsets of short- and long-period Cepheids. The results on the slopes are summarized in Table 5.

By taking into account the slopes listed in Tables 4 and 5, we reach the conclusion that the SMC Cepheids also indicate nonlinear *P–L* relations. In particular, data plotted in Figure 4 display a reasonable agreement between the observed slopes $b_{\rm all}$ and the predicted slopes for 12+log(O/H) = 8.17, whereas the observed $b_{\rm short}$ values are systematically flatter, and the observed $b_{\rm long}$ values are systematically steeper than current predictions.

2.3. Milky Way and M31

The published slopes for the MW and the M31 variables were estimated over the entire period range. Here, we only wish to note that the Galactic slopes determined by Benedict et al. (2007, hereinafter Be07) using trigonometric parallaxes, by Fouqué et al. (2007, hereinafter Fo07) using distances based on different methods and by Groenewegen (2008, hereinafter Gr08), who adopted a revised projection factor p to estimate the distances based on the Baade–Wesselink method, are significantly flatter than those found by STR04. The slopes we found for the Galactic and the M31 fundamental Cepheids are listed in Table 5. In the former case, we adopted *BVI* magnitudes from Berdnikov et al. (2000), *JK* magnitudes from Berdnikov et al. (1996), reddenings and distances from Fo07 and Gr08 (74 Cepheids, $0.6 \leqslant \log P \leqslant 1.8$). Note that the quoted authors use the extinctions provided by Laney & Caldwell (2007), the reddening law by Cardelli et al. (1989) and total to selective absorption ratios of $R_V = 3.23$ (Fo07) and of 3.3 (Gr08), respectively. In the following, we adopt $R_V = 3.23$ ($A_V/(A_V - A_I) = 2.55$, the same value adopted by the OGLE project). For the M31 variables, we adopted the sample investigated by Tammann et al. 2008, hereinafter TSR08), but the observed magnitudes were not unreddened with reddening corrections based on the Galactic Cepheids.

Table 4
Published Slopes (b) for Observed P–L Relations

Galaxy	Met.	log P	$b(B)$	$b(V)$	$b(I)$	$b(J)$	$b(K_s)$	Ref.[a]
LMC	8.34	0.4–2.0	-2.34 ± 0.04	-2.70 ± 0.03	-2.95 ± 0.02	...	...	(1)
LMC	"	0.4–1.0	-2.68 ± 0.08	-2.96 ± 0.06	-3.10 ± 0.04	...	...	(")
LMC	"	1.0–2.0	-2.15 ± 0.13	-2.57 ± 0.10	-2.82 ± 0.08	...	...	(")
LMC	"	0.4–2.0	...	...	...	-3.15 ± 0.05	-3.28 ± 0.04	(2)
LMC	"	0.4–1.7	-2.39 ± 0.04	-2.73 ± 0.03	-2.96 ± 0.02	-3.14 ± 0.03	-3.23 ± 0.03	(3)
LMC	"	0.4–1.0	-2.63 ± 0.07	-2.90 ± 0.05	-3.07 ± 0.04	-3.24 ± 0.04	-3.29 ± 0.04	(4)
LMC	"	1.0–1.7	-2.40 ± 0.19	-2.76 ± 0.14	-2.95 ± 0.10	-3.04 ± 0.15	-3.21 ± 0.14	(")
SMC	7.98	0.4–1.7	-2.22 ± 0.05	-2.59 ± 0.05	-2.86 ± 0.04	...	...	(5)
SMC	"	0.4–1.0	-2.33 ± 0.10	-2.58 ± 0.09	-2.82 ± 0.07	...	...	(")
SMC	"	1.0–1.7	-2.35 ± 0.22	-2.79 ± 0.18	-3.06 ± 0.13	...	...	(")
MW	8.60	0.6–1.9	-2.69 ± 0.09	-3.09 ± 0.09	-3.35 ± 0.08	...	...	(6)
MW	"	0.6–1.7	-2.29 ± 0.09	-2.68 ± 0.08	-2.98 ± 0.07	-3.19 ± 0.07	-3.37 ± 0.06	(7)
MW	"	0.6–1.8	...	-2.60 ± 0.09	...	...	-3.50 ± 0.08	(8)
MW	"	0.6–1.6	...	-2.43 ± 0.12	-2.81 ± 0.11	...	-3.32 ± 0.12	(9)
M31	8.68	0.4–1.6	-2.55	-2.92 ± 0.21	...	...	...	(10)

Notes. The galaxy metallicity in the second column is the galaxy nebular abundance 12+log(O/H) in the new scale.
[a] **References.** (1) Sandage et al. (2004, STR04) using OGLE (Udalski et al. 1999a) *BVI* magnitudes plus additional data from different sources. (2) Persson et al. (2004, Pe04) using 2MASS near-infrared magnitudes. (3) Fouqué et al. (2007, Fo07) using OGLE and Pe04 magnitudes plus additional near-infrared data. (4) Ngeow et al. (2008, NKN08) using the same data set used by Fo07. (5) Sandage et al. (2009) using OGLE (Udalski et al. 1999b) *BVI* magnitudes. (6) STR04 using either cluster or Baade–Wesselink distances to Galactic Cepheids. (7) Fo07 using revised Baade-Wesselink distances to selected Galactic Cepheids. (8) Groenewegen (2008, Gr08) using revised Baade–Wesselink distances to selected Galactic Cepheids. (9) Benedict et al. (2007, Be07) using trigonometric parallaxes to selected Galactic Cepheids. The K-band data are in the CIT near-infrared system. (10) Tammann et al. (2008, TSR08) using Cepheids with visual amplitude $A_V > 0.8$ mag, observed by Vilardell et al. (2007), and individual reddenings based on the Galactic P–C relation.

Table 5
Slopes (b) of the Observed P–L Relations Determined in the Present Paper

Galaxy	Met.	log P	$b(B)$	$b(V)$	$b(I)$	$b(J)$	$b(K_s)$	Notes[a]
SMC	7.98	0.5–2.0	-2.45 ± 0.05	-2.80 ± 0.08	-3.02 ± 0.07	...	...	(1)
SMC	"	0.5–1.0	-2.28 ± 0.15	-2.56 ± 0.12	-2.80 ± 0.09	...	...	(")
SMC	"	1.0–2.0	-2.50 ± 0.17	-2.89 ± 0.13	-3.15 ± 0.12	-3.41 ± 0.19	-3.56 ± 0.18	(")
MW	8.60	0.6–1.8	-2.29 ± 0.10	-2.71 ± 0.10	-3.04 ± 0.09	-3.29 ± 0.09	-3.45 ± 0.09	(2)
MW	"	0.6–1.8	-2.32 ± 0.10	-2.74 ± 0.12	-3.07 ± 0.11	-3.31 ± 0.09	-3.47 ± 0.09	(3)
M31	8.68	0.5–1.6	-2.29 ± 0.15	-2.72 ± 0.11	...	...	...	(4)

Note. The metallicity listed in the second column is the galaxy nebular abundance 12+log(O/H) in the new metallicity scale.
[a] Notes: (1) OGLE (Udalski et al. 1999b) magnitudes plus additional Cepheids from Caldwell & Coulson (1984, *BVI*) and Laney & Stobie (1986, *JK*). (2) Entire sample of Galactic Cepheids with distances measured by Fo07. (3) Entire sample of Galactic Cepheids with distances measured by Gr08. (4) Cepheids with visual amplitude $A_V > 0.8$ mag, observed by Vilardell et al. (2007), but without reddening correction.

We decided to follow this approach because, as noted by TSR08, the assumption that the M31 Cepheids obey the Galactic period–color relation gives the unpleasant result of individual reddenings which increase with the period. Note that the original near-infrared magnitudes of SMC and MW Cepheids have been transformed into the Two Micron All Sky Survey (2MASS) photometric system by using the transformations provided by Fo07.

The occurrence of a nonlinear P–L relation can be barely detected for MW and M31 Cepheids, likely due to the uncertainties on individual distances and on reddening corrections. However, it is worth noting that our overall P–L relations are flatter than those determined by STR04 and TSR08, but our Galactic $b_{\rm all}$ slopes are almost identical to those provided by Fo07 and Gr08. Data plotted in Figure 5 show that all the $b_{\rm all}$ values, apart from those determined by STR04, for Cepheids with a solar-like chemical composition are in reasonable agreement with predicted slopes for metal-rich chemical compositions, namely 12+log(O/H) = 8.58 (solid line) and 12+log(O/H) = 8.89 (dashed line).

In conclusion, the predicted nonlinear feature of the optical P–L relations seems verified by LMC and SMC Cepheids, but with opposite slope differences between short- and long-period variables. Moreover, we found that the observed *overall* slopes for the Magellanic, MW, and M31 Cepheids agree quite well with the predicted values and suggest a flattening toward more metal-rich chemical compositions. This finding is at variance with the steepening found by TSR08, STR08, and by Sandage & Tammann (2008, hereinafter ST08) and it will be discussed in the next section.

3. DEPENDENCE OF THE P–L SLOPE ON THE CEPHEID METALLICITY

In Table 6, we list the observed $b(V)$ and $b(I)$ slopes of single-fit P–L relations according to TSR08 and to Saha et al. (2006, hereinafter STT06). The left panels of Figure 6 show the TSR08 slopes (filled circles) versus the galaxy metallicity, together with the means (open circles) of metal-poor (M-P) and metal-rich (M-R) galaxies from STT06 according to TSR08. These

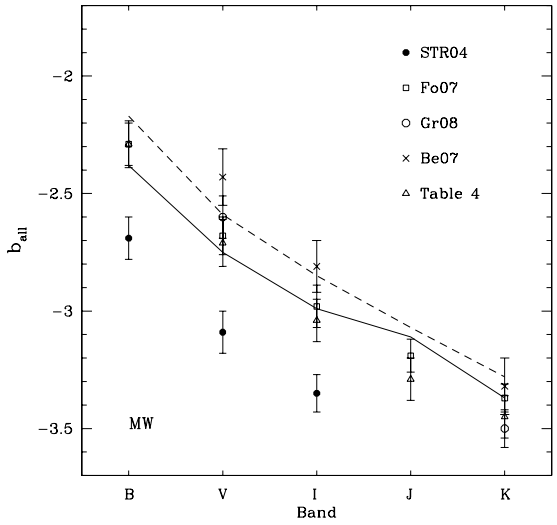

Figure 5. Comparison between observed slopes of the Galactic *P–L* relations (open symbols) and the predicted values for a chemical composition of 12+log(O/H) = 8.58 (solid line) and 12+log(O/H) = 8.89 (dashed line).

Table 6
Slopes $b(V)$ and $b(I)$ for Observed *P–L* Relations Provided by Tammann et al. (2008, TSR08) and by Saha et al. (2006, STT06)

Galaxy	Met.	$b(V)$	$b(I)$	Notes[a]
		TSR08		
N3351	8.85	-3.12 ± 0.39	-3.38	
N4321	8.74	-3.17 ± 0.34	-3.43	
N0224	8.68	-2.92 ± 0.21	...	
MW	8.60	-3.09 ± 0.09	-3.35	
LMC	8.34	-2.70 ± 0.03	-2.95	
N6822	8.14	-2.49 ± 0.01	-2.81	
N3109	8.06	-2.13 ± 0.18	-2.40	
SMC	7.98	-2.59 ± 0.05	-2.86	
IC1613	7.86	-2.67 ± 0.12	-2.80	
WLM	7.74	-2.52 ± 0.15	-2.74	
Sext(A+B)	7.52	-1.59 ± 0.39	-1.47	(1)
M-P	8.36	-2.69 ± 0.12	-2.97	(2)
M-R	8.75	-2.88 ± 0.13	-3.13	(3)
		STT06		
N3351	8.85	-2.52	-3.01	
N4548	8.85	-1.35	-2.31	
N3627	8.80	-2.28	-2.64	
N4535	8.77	-2.85	-3.05	
N4321	8.74	-3.02	-3.32	
N5457i	8.70	-2.36	-2.68	(4)
N1425	8.67	-1.85	-2.13	
N3198	8.43	-2.36	-2.60	
N0925	8.40	-2.78	-2.88	
N2541	8.37	-2.53	-3.26	
N1326A	8.37	-2.75	-2.99	
N0300	8.35	-2.79	-2.95	
N3319	8.28	-2.41	-3.11	
N5457o	8.23	-2.13	-2.71	(5)

Note. The galaxy metallicity in the second column is the nebular oxygen abundance 12+log(O/H) in the new scale.
[a] Notes: (1) The entire sample of Cepheids in the two galaxies Sextans A and Sextans B is combined in a single relation. (2) Mean values of the metal-poor [12+log(O/H) < 8.45] galaxies from STT06. (3) Mean values of the metal-rich [12+log(O/H) > 8.65] galaxies from STT06. (4) Inner field Cepheids. (5) Outer field Cepheids.

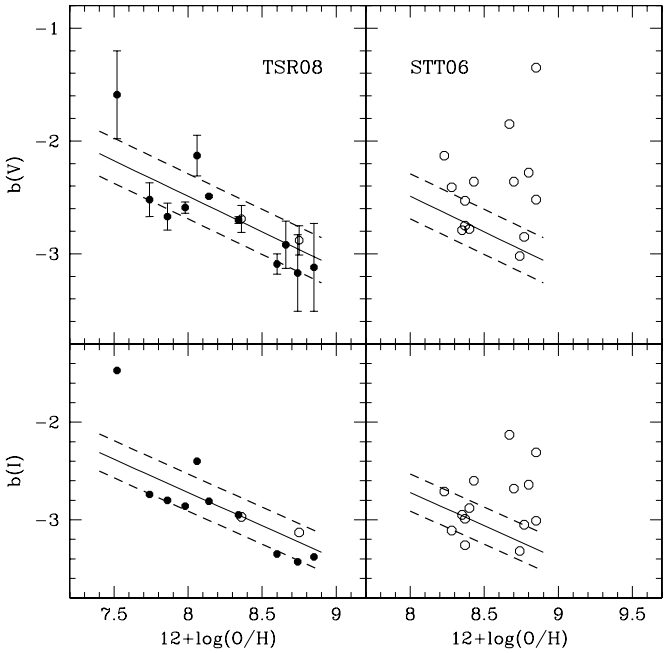

Figure 6. Left: observed $b(V)$ and $b(I)$ slopes according to TSR08 as a function of the galaxy metal content. The open circles are the mean values for the metal-poor and the metal-rich galaxies according to STT06. The solid lines are the least square fits to the data, while the dashed lines display the 1σ dispersion around the fit (see text). The couple Sextans (A+B) were not included in the fit. Right: observed $b(V)$ and $b(I)$ slopes for all the galaxies studied by STT06. Both solid and dashed lines have the same meaning as in the left panels.

data show an indisputable steepening of the *P–L* relation with increasing galaxy metal abundance. We excluded the couple Sextans (A+B), which has the lowest oxygen abundance, since their *P–L* relations are based on a few Cepheids ($N_{\rm Ceph} \leqslant 10$), and we found

$$b(V) = -2.70–0.63[\log(\mathrm{O/H}) + 3.66] \quad (2)$$

$$b(I) = -2.95–0.68[\log(\mathrm{O/H}) + 3.66] \quad (3)$$

with standard deviations around the fit of $\sigma_{b(V)} = 0.20$ and $\sigma_{b(I)} = 0.19$, respectively. However, the right panels of Figure 6 show quite clearly that such a trend can hardly explain the location on this plane of several metal-rich galaxies studied by STT06, which actually present quite flat *P–L* relations deviating more than 2σ from the TSR08 relations.

To shed new light on this interesting evidence, we took into account all the galaxies with Cepheid photometry available in the recent literature and performed a new estimate of the slope of the *P–L* relations. In particular, we adopted all the fundamental variables with $0.5 \leqslant \log P \leqslant 2.0$, the observed magnitudes were selected adopting a 2σ clipping, and we assumed that the reddening is independent of the Cepheid period. Concerning the metallicity of these extragalactic variables, we remind that they are generally based on the nebular oxygen abundance of the host galaxy and that the abundance scale provided by Zaritsky et al. (1994, hereinafter ZKH) has been recently revised by Sakai et al. (2004, hereinafter Sa04) and by STT06. Their data concerning *old* and *new* values are listed in Table 7 and are plotted in Figure 7 together with the polynomial regression which has been used in the current paper to transform additional abundances in the ZKH scale into the new abundance scale.

The full list of the observed $b(V)$ and $b(I)$ slopes derived in the present paper is given in Columns 3 and 4 of Table 8, together

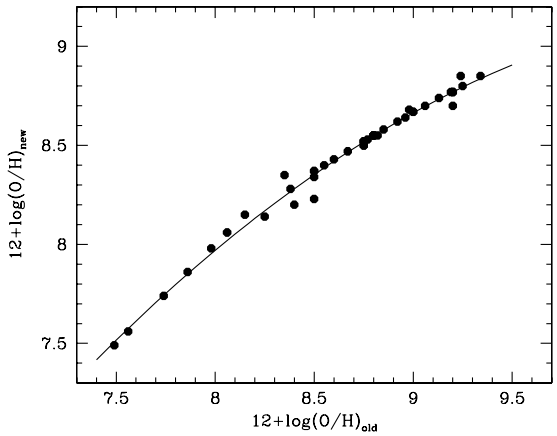

Figure 7. Relation between new and old oxygen abundances given by Sakai et al. (2004) and by STT06. The solid line is the polynomial fit adopted in the current paper to derive the chemical compositions listed in Table 7.

Table 7
Galaxy Metal Abundances in the Notation 12+log(O/H)

Galaxy	Ref.[a]	Met_{old}	Met_{new}
IC1613	Sa04	7.86 ± 0.50	7.86
IC4182	STT06	8.40 ± 0.20	8.20
LMC	Sa04	8.50 ± 0.08	8.34
N0224	STT06	8.98 ± 0.15	8.68
N0300	STT06	8.35 ± 0.15	8.35

Notes. The values marked with an asterisk have been estimated using the polynomial regression presented in Figure 7 (see the text for more details).

[a] **References.** Scowcroft et al. 2009; Riess et al. 2009, Ri09; McCommas et al. 2009, hereinafter McC09.

(This table is available in its entirety in a machine-readable form in the online journal. A portion is shown here for guidance regarding its form and content.)

with the galaxy metallicity in the new scale and the appropriate reference. Several galaxies were either observed or revised by the "Extragalactic Distance Scale Key Project" (hereinafter KP) or by the "Type Ia Supernova Calibration Project" (hereinafter SNP), or by other authors and we give the results for each galactic sample.

Looking at the slopes listed in Table 8, we note that different photometric data for the same galaxy may lead to quite different slopes, in particular for the galaxies with few Cepheids. This is an unpleasant result, but the real gist of the matter is shown in Figure 8, where all our *P–L* slopes are plotted as a function of the galaxy metal content. In spite of the large spread of the *P–L* slopes at fixed metal abundance, we are facing the evidence that all the Cepheids suggest a puzzling parabolic metallicity dependence with a sort of "turn-over" around 12+log(O/H) $\sim$ 8.2. The less metal abundant galaxies show a flattening of the *P–L* relation with decreasing metallicity, whereas the more metal abundant galaxies show an opposite trend. Note that the most metal-poor galaxy (12+log(O/H) $\sim$ 7.5) plotted in the above figure is Sextans A (see also Table 8).

In order to overcome possible spurious effects due to limited samples, we only took into account galaxies with at least 20 Cepheids (filled circles in Figure 8), and we compared the observed slopes with three selected metallicity dependences.

1. *Steady steepening of the P–$L_{V,I}$ relations with increasing metal content.* By using the metallicity dependence of

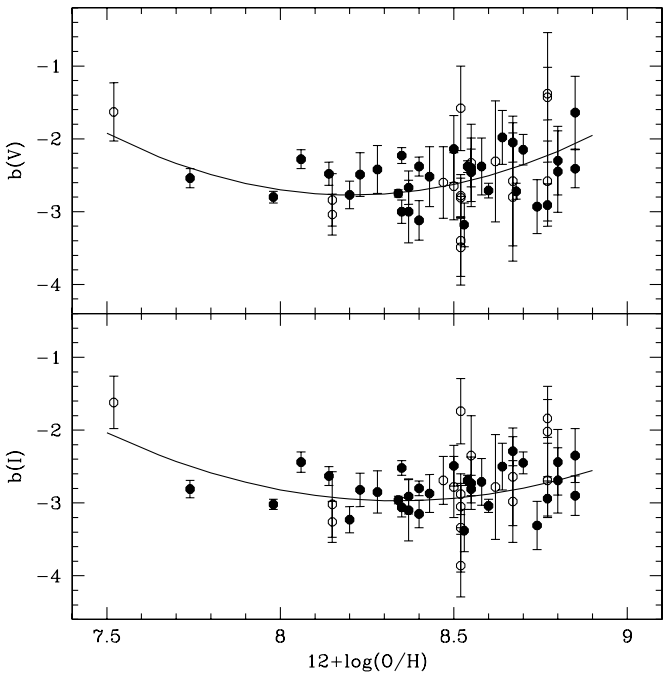

Figure 8. Observed $b(V)$ and $b(I)$ slopes listed in Table 8, as a function of the galaxy metal content. Filled circles display slopes based on at least 20 Cepheids. The solid lines depict the quadratic fit to the data.

Table 8
Slopes $b(V)$ and $b(I)$ of Observed *P–L* Relations Estimated Using Cepheids with $0.5 \leqslant \log P \leqslant 2.0$

Galaxy	Met.	$b(V)$	$b(I)$	$\beta(WVI)$	Ref.[a]
IC1613	7.86	-2.72 ± 0.13	-2.92 ± 0.10	-3.34 ± 0.06	(1, 2)
IC4182	8.20	-2.80 ± 0.17	-3.23 ± 0.18	-3.93 ± 0.26	Ka03
IC4182	8.20	-2.60 ± 0.17	-2.93 ± 0.18	-3.43 ± 0.26	KPr
IC4182	8.20	-2.73 ± 0.16	-3.15 ± 0.17	-3.81 ± 0.19	STT06
LMC	8.34	-2.70 ± 0.03	-2.95 ± 0.02	-3.37 ± 0.03	STR04
MW	8.60	-2.71 ± 0.10	-3.04 ± 0.09	-3.52 ± 0.12	Table 5
N0055	...	-2.29 ± 0.15	-2.56 ± 0.12	-2.90 ± 0.13	(3, 4)
N0224	8.68	-2.72 ± 0.11	...	...	Table 5
N0247*	...	-2.34 ± 0.19	-2.71 ± 0.16	-3.39 ± 0.35	(5, 6, 7)
N0300	8.35	-3.00 ± 0.11	-3.12 ± 0.12	-3.29 ± 0.12	(8, 9)

Notes. The subscripts i and o refer either to the inner field or to the outer field Cepheids. The galaxies with a Cepheid number smaller than 20 are marked with an asterisk. Column 5 gives the slope $\beta(WVI)$ of the observed *P–WVI* relations discussed in Section 4.

[a] **References.** [KP] galaxies download from the KP Web page. [STT06] SNP galaxies revised by Saha et al. (2006). [Ka03] KP and SNP galaxies revised by Kanbur et al. (2003). [KPr] KP and SNP galaxies revised by the KP group. (1) Udalski et al. 2001; (2) Pietrzynski et al. 2006a; (3) Pietrzynski et al. 2006b; (4) Gieren et al. 2008a; (5) García-Varela et al. 2008; (6) Madore et al. 2009; (7) Gieren et al. 2009; (8) Gieren et al. 2004; (9) Gieren et al. 2005; (10) Scowcroft et al. 2009; (11) Riess et al. 2009; (12) Leonard et al. 2003; (13) Macri et al. 2001; (14) McCommas et al. 2009; (15) Pietrzynski et al. 2006c; (16) Soszynski et al. 2006; (17) Tanvir et al. 1999; (18) Riess et al. 2005; (19) Stetson & Gibson 2001; (20) Macri et al. 2006; (21) Newman et al. 2001.; (22) Gibson & Stetson 2001; (23) Ferrarese et al. 2007; (24) Thim et al. 2003; (25) Pietrzynski et al. (2004); (26) Gieren et al. (2006); (27) Piotto et al. (1994); (28) Dolphin et al. (2003); (29) Pietrzynski et al. (2007); (30) Gieren et al. (2008b).

(This table is available in its entirety in a machine-readable form in the online journal. A portion is shown here for guidance regarding its form and content.)

Equations (2) and (3) and the ensuing zero points of the $b(V)$ and of the $b(I)$ relations (-2.50 ± 0.28 and -2.89 ± 0.26), the

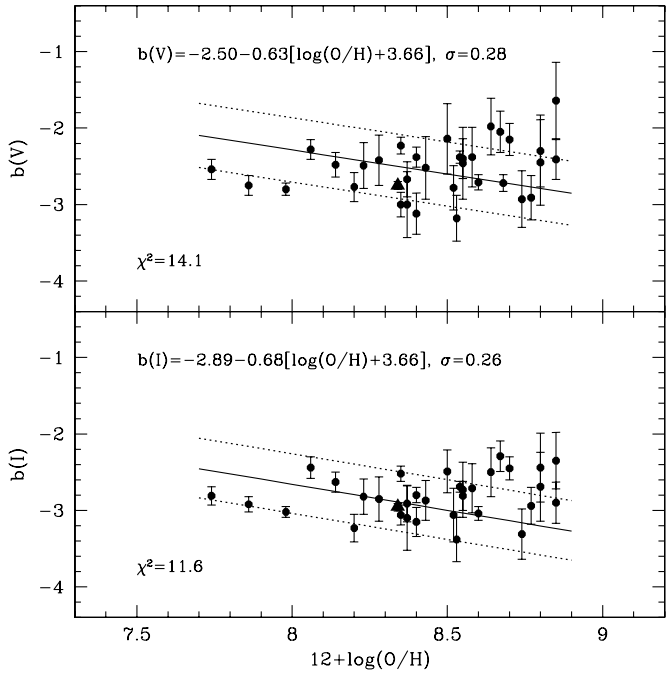

Figure 9. Same as Figure 8, but using only galaxies with at least 20 Cepheids. The solid lines are drawn according to the labeled relations, which adopt the metallicity dependence of Equations (2) and (3), while the dotted lines depict the 1.5σ dispersion around them. The χ^2 values are derived by comparison of observed frequencies with those predicted by a normal distribution (see the text).

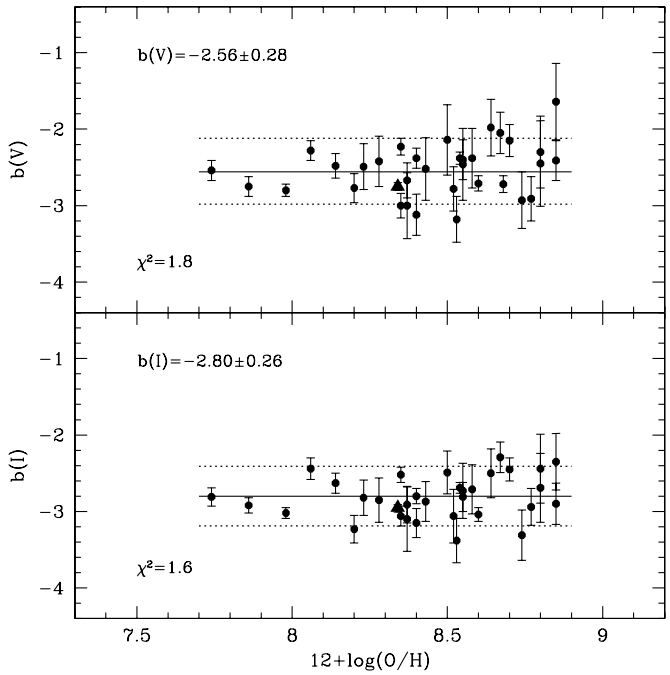

Figure 10. Same as in Figure 9, but assuming no dependence of the $b(V)$ and of the $b(I)$ slopes on the galaxy metal abundance.

slopes plotted in Figure 9 show that several metal-rich galaxies deviate more than $+1.5\sigma$ (dotted line). The χ^2 test on the observed frequencies in the intervals $<-1.5\sigma$, -1.5σ to 0, 0 to $+1.5\sigma$, and $>+1.5\sigma$ when compared with a normal distribution gives $\chi^2_{b(V)} = 14.1$ and $\chi^2_{b(I)} = 11.6$. These values, for 3 degrees of freedom, mean that the above hypothesis can be discarded with a confidence level of 99%.

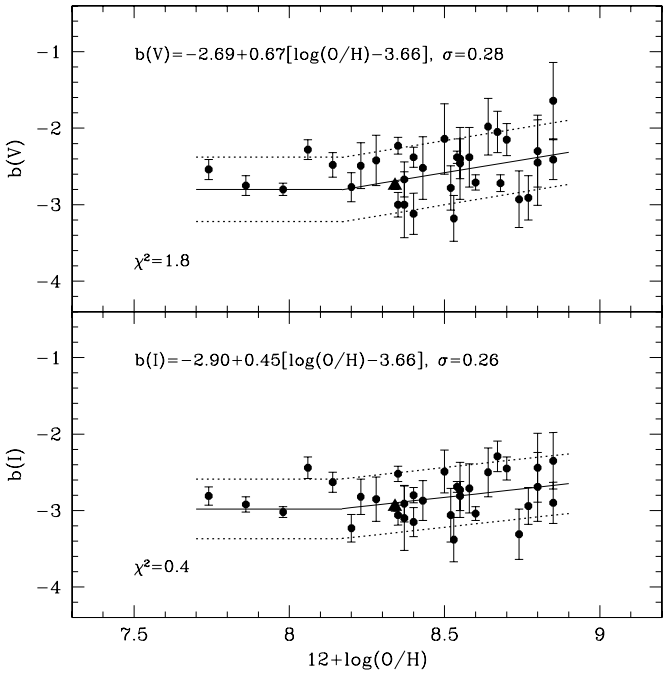

Figure 11. Same as in Figure 9, but assuming the metallicity dependence predicted by the pulsation models for chemical compositions with $\log(Z/X) \geqslant -2.27$ and a constant slope for $\log(Z/X) < -2.27$.

2. *Null hypothesis.* By assuming no dependence of the slopes on the metal content (see Figure 10) and by using the mean values $b(V) = -2.56 \pm 0.28$ and $b(I) = -2.80 \pm 0.26$, the χ^2 test gives $\chi^2_{b(V)} = 1.8$ and $\chi^2_{b(I)} = 1.6$. This means that we can accept the hypothesis with a confidence level of 62% and of 67%, respectively.

3. *Trend predicted by pulsation models.* Figure 11 shows that the slope of the P–L_V and of the P–L_I relation becomes shallower with increasing metal content for 12+log(O/H) $\geqslant$ 8.17 and constant for lower metal abundances as suggested by the pulsation models. In this case, the χ^2 test gives $\chi^2_{b(V)} = 1.8$ and $\chi^2_{b(I)} = 0.6$, i.e., the theoretical hypothesis can be accepted with a confidence level of 62% and 92%, respectively.

In conclusion, the slopes of the observed P–L_V and P–L_I relations seem to exclude the steepening with increasing metallicity suggested by TSR08. Current findings suggest that the slopes are either metallicity independent or they follow the metallicity dependence predicted by the pulsation models. In the latter case, the use of these P–L relations for distance determinations *could* require specific corrections to account for the difference in the slope. This issue is discussed in the next section, where we show the impact of the P–L slopes on the Cepheid distance scale.

4. INTRINSIC FEATURES OF THE P–W RELATIONS

The fiducial P–L relations based on the unreddened magnitudes of the LMC Cepheids can be used to derive the LMC-relative apparent distance modulus $\delta\mu_i$ of a given variable and the use of two or more passbands provides the opportunity to estimate the reddening, e.g., $\delta\mu_B - \delta\mu_V = A_B - A_V = E(B-V)$. Then, the use of a wavelength-dependent extinction law yields the correction for the selective extinction in the different bands, and eventually the LMC-relative true distance modulus $\delta\mu_0$.

This approach is equivalent to the method based on the so-called Wesenheit functions; since the early papers on Cepheid

Table 9
Predicted Slopes $\beta(W)$ of the *P–W* Relations Given by the Intensity-weighted Mean Magnitudes of Fundamental Pulsators with $0.5 \leqslant \log P \leqslant 2.0$ and $Z = 0.001$–0.04

Met.	$\beta(WBV)$	$\beta(WVI)$	$\beta(WJK_s)$
7.56	-3.80 ± 0.03	-3.35 ± 0.03	-3.37 ± 0.03
8.17	-3.83 ± 0.02	-3.37 ± 0.03	-3.39 ± 0.03
8.47	-3.81 ± 0.03	-3.31 ± 0.04	-3.38 ± 0.03
8.58	-3.80 ± 0.03	-3.24 ± 0.04	-3.37 ± 0.04
8.89	-3.82 ± 0.03	-3.22 ± 0.03	-3.36 ± 0.03
9.10	-3.77 ± 0.03	-3.20 ± 0.03	-3.31 ± 0.03
9.22	-3.76 ± 0.03	-3.23 ± 0.03	-3.32 ± 0.03

Note. The metallicity in the first column is the oxygen abundance 12+log(O/H) listed in Table 3.

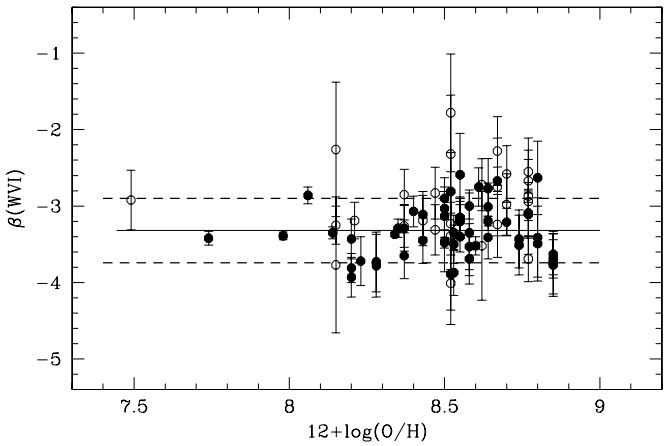

Figure 12. Slopes of the observed *P–WVI* relations for the same galaxies plotted in Figure 8. The solid and dashed lines refer to the mean value and to the 1.5σ dispersion, respectively.

investigations (see Madore 1982; Madore & Freedman 1991) the problem of dust extinction is generally accounted for using the Cepheid colors to derive extinction-free magnitudes (e.g., $WBV = V - R_V(B - V)$, where R_V is the visual extinction-to-reddening ratio $A_V/E(B - V)$) and to use them in period–Wesenheit (*P–W*) relations that are independent of reddening. We note that the effect of the extinction is similar to the one produced by the finite width of the instability strip, therefore, the scatter around the *P–W* relations is smaller than in any observed *P–L* relation. Thus, we are facing the circumstantial evidence that the dependence on metallicity of the slope of a monochromatic *P–L* relation could have a minimal impact upon the distance scale if the combination of different magnitudes and colors leads to a metallicity independent slope for the *P–W* relations.

On the theoretical side, the bolometric light curves provided by the nonlinear approach, once transformed into the observational plane by using model atmospheres, provide the amplitudes in the various spectral bands and, after a time integration, the predicted mean magnitudes of the pulsators. In Table 9, we give the predicted slope $\beta(W)$ of selected *P–W* relations ($W = \alpha + \beta \log P$) for fundamental pulsators with $0.5 \leqslant \log P \leqslant 2.0$, based on intensity-weighted mean magnitudes $\langle M_i \rangle$ and colors $[\langle M_i \rangle - \langle M_j \rangle]$ and on the Cardelli et al. (1989) reddening law with $R_V = 3.23$. Note that the original near-infrared magnitudes of our models, which are in the Bessell & Brett photometric system, have been transformed into the 2MASS system using the conversion relations adopted by Fo07.

The predicted *P–W* relations are quite tight and show several additional undeniable advantages:

1. They are almost independent of the pulsator distribution within the instability strip. For this reason, in Table 9 we also give the results for the $Z = 0.001$ models.
2. They are almost linear over the entire period range.
3. The effects of the mixing-length, l/H_p, at fixed metal, *Z*, and helium, *Y*, content on both the slope and zero point are negligible.
4. The adopted helium content *Y*, at fixed metal content *Z* and mass–luminosity relation, only affects the zero point of the relations.
5. Their slopes turn out to be almost independent of the chemical composition.

The above issues have been discussed in our previous papers (see Fiorentino et al. 2007; Bono et al. 2008, and references therein), where we showed that the impact of the metallicity on the *P–W* zero point also depends on the adopted Wesenheit function. Here, we test these predictions by directly using Cepheid observations.

First, the linearity of the predicted *P–W* relations agrees with the recent results by Ngeow & Kanbur (2005) and by Ngeow et al. (2005) from measurements of LMC Cepheids and, as recently discussed by Madore & Freedman (2009), is expected even though the underlying monochromatic *P–L* relations are nonlinear. Second, the slope of our own LMC relations

$$WBV = 16.04(\pm 0.04) - 3.82(\pm 0.06) \log P, \quad (\sigma = 0.19) \tag{4}$$

$$WVI = 15.91(\pm 0.03) - 3.37(\pm 0.03) \log P, \quad (\sigma = 0.09) \tag{5}$$

$$WJK_s = 15.97(\pm 0.07) - 3.45(\pm 0.06) \log P, \quad (\sigma = 0.10) \tag{6}$$

are quite consistent with the predicted values listed in Table 9. Finally, previous studies have already shown that the slope of the *P–W* relations defined by Cepheids in the Galaxy (Be07; van Leeuwen et al. 2007), in metal-poor galaxies (Pietrzynski et al. 2007), and in metal-rich ones (Riess et al. 2009, hereinafter Ri09) agrees quite well with the slope of the LMC variables. This result is supported by the $\beta(WVI)$ values derived in the present paper, which are listed in the last column of Table 8 and are plotted versus the galaxy oxygen abundance in Figure 12. In particular, we find that only the slopes based on small Cepheid samples ($N_{\rm Cep} < 20$, open circles) deviate more than 2σ from the weighted mean $\beta(WVI) = -3.32 \pm 0.21$, which in turn is practically identical to the LMC value. Moreover, the new slopes of the observed *P–WBV* and *P–WJK*$_s$ relations listed in Table 10 are also very similar to the LMC values. There are only two exceptions, namely Sextans A and the outer region of NGC 598.

In conclusion, empirical findings strongly support the use of the *P–W* relations based on LMC Cepheids to derive the LMC-relative true distance modulus of individual Cepheids, provided that the metallicity dependence of the zero point of the different *P–W* relations, if present, is taken into account.

We recall that independent observations suggest either a negligible metallicity effect on the Cepheid distance scale

Table 10
Observed Slopes of the *P–WBV* and *P–WJK$_s$* Relations, as Derived in the Present Paper for Cepheids with $0.5 \leqslant \log P \leqslant 2.0$

Galaxy	Met.	$\beta(WBV)$	$\beta(WJK_s)$
IC1613	7.86	...	-3.27 ± 0.19
IC1613[a]	7.86	-3.70 ± 0.15	...
LMC	8.34	-3.82 ± 0.04	-3.45 ± 0.06
MW	8.60	-4.04 ± 0.12	-3.54 ± 0.10
N0055	...	...	-3.19 ± 0.18
N0224	8.68	-3.99 ± 0.10	...
N0247	...	...	-3.26 ± 0.15
N0300	8.35	-4.04 ± 0.28	-3.12 ± 0.25
N0598i	8.58	-3.23 ± 0.30	...
N0598o	8.21	-3.08 ± 0.30	...
N4258i	8.64	-3.77 ± 0.10	...
N4258o	8.50	-3.97 ± 0.10	...
N6822	8.14	...	-3.12 ± 0.14
SextA	7.49	-2.41 ± 0.38	...
SextB	7.56	-3.96 ± 0.40	...
SMC	7.98	-3.94 ± 0.05	-3.29 ± 0.16
WLM	7.74	...	-3.17 ± 0.19

Note. [a] Data from Antonello et al. (2006).

Table 11
Mean LMC-relative True Distance Moduli of Canonical Fundamental Pulsators with $0.5 \leqslant \log P \leqslant 2.0$ and $Z = 0.001$–0.04 Based on the Intensity-averaged Magnitudes of the Pulsators and on the Observed LMC *P–W* Relations Discussed in the Text

Met.	Y	$\delta\mu_0(WBV)$	$\delta\mu_0(WVI)$	$\delta\mu_0(WJK_s)$
		$\log L/L_{\rm can} = 0$		
7.56	0.24	-18.16 ± 0.05	-18.68 ± 0.11	-18.65 ± 0.10
8.17	0.25	-18.46 ± 0.06	-18.75 ± 0.11	-18.75 ± 0.09
8.48	0.25	-18.72 ± 0.05	-18.77 ± 0.09	-18.79 ± 0.08
8.58	0.26	-18.72 ± 0.07	-18.73 ± 0.12	-18.74 ± 0.10
8.88	0.25	-18.99 ± 0.08	-18.70 ± 0.10	-18.73 ± 0.08
8.89	0.26	-18.97 ± 0.07	-18.74 ± 0.10	-18.75 ± 0.08
8.90	0.28	-18.94 ± 0.08	-18.67 ± 0.12	-18.73 ± 0.08
8.92	0.31	-18.90 ± 0.04	-18.65 ± 0.11	-18.64 ± 0.08
9.08	0.275	-19.05 ± 0.07	-18.72 ± 0.09	-18.66 ± 0.09
9.10	0.31	-19.00 ± 0.07	-18.64 ± 0.09	-18.59 ± 0.08
9.12	0.335	-18.98 ± 0.07	-18.64 ± 0.08	-18.57 ± 0.08
9.19	0.25	-19.20 ± 0.08	-18.82 ± 0.07	-18.70 ± 0.05
9.22	0.29	-19.13 ± 0.06	-18.77 ± 0.06	-18.65 ± 0.07
9.25	0.33	-19.07 ± 0.08	-18.71 ± 0.06	-18.58 ± 0.08
		$\log L/L_{\rm can} = 0.20$		
8.17	0.25	-18.27 ± 0.06	-18.55 ± 0.11	-18.57 ± 0.09
8.48	0.25	-18.54 ± 0.04	-18.57 ± 0.09	-18.61 ± 0.08
8.88	0.28	-18.75 ± 0.07	-18.47 ± 0.10	-18.55 ± 0.08

Note. The metallicity in the first column is the oxygen abundance 12+log(O/H) listed in Table 3.

Table 12
Internal Differences Among the LMC-relative True Distance Moduli Listed in Table 11

Met.	Y	$\Delta(WBV - WVI)$	$\Delta(WBV - WJK_s)$	$\Delta(WVI - WJK_s)$
		$\log L/L_{\rm can} = 0$		
7.56	0.24	$+0.42 \pm 0.10$	$+0.49 \pm 0.10$	$+0.03 \pm 0.10$
8.17	0.25	$+0.26 \pm 0.11$	$+0.29 \pm 0.08$	0 ± 0.11
8.48	0.25	$+0.04 \pm 0.09$	$+0.07 \pm 0.07$	$+0.03 \pm 0.08$
8.58	0.26	$+0.01 \pm 0.11$	$+0.02 \pm 0.09$	$+0.01 \pm 0.11$
8.88	0.25	-0.29 ± 0.09	-0.26 ± 0.07	$+0.03 \pm 0.08$
8.89	0.26	-0.23 ± 0.10	-0.22 ± 0.07	$+0.01 \pm 0.10$
8.90	0.28	-0.29 ± 0.11	-0.21 ± 0.07	$+0.06 \pm 0.10$
8.92	0.31	-0.25 ± 0.10	-0.26 ± 0.07	-0.01 ± 0.10
9.08	0.275	-0.34 ± 0.08	-0.39 ± 0.06	-0.06 ± 0.08
9.10	0.31	-0.36 ± 0.08	-0.41 ± 0.07	-0.05 ± 0.09
9.12	0.335	-0.34 ± 0.08	-0.41 ± 0.07	-0.07 ± 0.09
9.19	0.25	-0.37 ± 0.06	-0.50 ± 0.05	-0.12 ± 0.06
9.22	0.29	-0.36 ± 0.06	-0.50 ± 0.06	-0.14 ± 0.07
9.25	0.33	-0.36 ± 0.06	-0.49 ± 0.07	-0.16 ± 0.07
		$\log L/L_{\rm can} = 0.20$		
8.17	0.25	$+0.26 \pm 0.10$	$+0.30 \pm 0.09$	$+0.02 \pm 0.09$
8.48	0.25	$+0.03 \pm 0.08$	$+0.08 \pm 0.09$	$+0.05 \pm 0.09$
8.88	0.28	-0.28 ± 0.08	-0.20 ± 0.07	$+0.08 \pm 0.09$

or that variables in metal-rich galaxies are, at fixed period, *brighter* than those in metal-poor galaxies (see, e.g., Sasselov et al. 1997; Kennicutt et al. 1998, 2003; Kanbur et al. 2003; Tammann et al. 2003; Sandage et al. 2004; Storm et al. 2004; Groenewegen et al. 2004; Sakai et al. 2004; Ngeow & Kanbur 2004; Pietrzynski et al. 2007). In the latter case, the various estimates of the parameter $\gamma = c/\delta\log Z$, where c is the size (in magnitude) of the metallicity correction and $\delta\log Z = \log Z_{\rm LMC} - \log Z_{\rm Ceph}$, depends on the wavelength but always give *negative* numbers, with an average value of approximately -0.27 mag dex^{-1} (see the discussion in Groenewegen 2008). However, recent spectroscopic iron-to-hydrogen [Fe/H] measurements of Galactic and Magellanic Cepheids (Romaniello et al. 2005, 2008; Groenewegen 2008) seem to suggest that the *P–L$_V$* relation becomes *fainter* with increasing metallicity. Current data provided no firm conclusion concerning the dependence of *P–L$_K$* relation on the metal content.

By using the pulsation models listed in Table 1, we can derive, by assuming that these are actual Cepheids located at the same distance ($\mu_0 = 0$) and with different chemical compositions, from Equations (4)–(6) their LMC-relative true distance moduli $\delta\mu_0(WBV)$, $\delta\mu_0(WVI)$, and $\delta\mu_0(WJK_s)$. By averaging the results over the period range $0.5 \leqslant \log P \leqslant 2.0$, we derived the values at $\log L/L_{\rm can} = 0$ and 0.2 (see Table 11). They clearly show that the $\delta\mu_0$ values mainly depend on the filter and on the $L/L_{\rm can}$ ratio. Moreover, the metallicity effect on $\delta\mu_0(WBV)$ is quite strong and at constant $L/L_{\rm can}$ ratio we found $\gamma(WBV) = -0.58(\pm0.03)$ mag dex^{-1}, where the error takes into account the different helium abundances at constant Z. On the other hand, the variations of $\delta\mu_0(WVI)$ and of $\delta\mu_0(WJK_s)$ are significantly smaller and both the extent and the sign of the metallicity effect seem to depend both on the helium content (at fixed Z), and on the adopted metallicity range (see also Section 5).

It is worth underlining that the *internal differences* among the various LMC-relative distance moduli listed in Table 12 depend on the metal content, but they are independent of the helium content (at fixed Z) and of the adopted $M\,L$ relation. Specifically, the differences $\Delta(WBV - WVI) = \delta\mu_0(WBV) - \delta\mu_0(WVI)$ and $\Delta(WBV - WJK_s) = \delta\mu_0(WBV) - \delta\mu_0(WJK_s)$ are quite sensitive to the metal content, and could provide a robust diagnostic to estimate the Cepheid metal content, since they are independent of uncertainties affecting reddening corrections.

On the observational side, let us use once again Equations (4)–(6) to derive the LMC-relative Cepheid distance moduli in external galaxies for which are available *BVIJK$_s$* data. We show in Table 13 that the *P–WVI* and *P–WJK$_s$* relations provide similar results, whereas the *P–WBV* relation, for galaxies more metal poor than the LMC, yields larger distances. As a whole, we found $\partial\Delta(WBV - WVI)/\partial\log(O/H) \sim -0.4$ mag

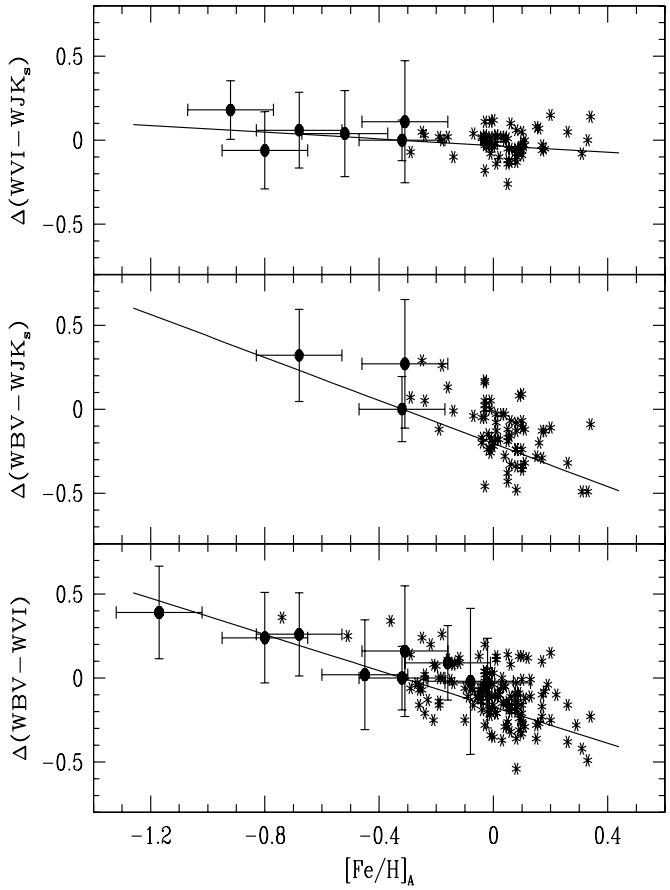

Figure 13. Metallicity dependence of the differences among LMC-relative distance moduli for the external galaxies listed in Table 13 and for the MW Cepheids with $\log P > 0.5$. For the external galaxies, we adopted [Fe/H] = log(O/H)+3.34 with a typical error of ±0.15 dex, while for the Galactic Cepheids we adopted the iron measurements provided by Andrievsky and collaborators ($[Fe/H]_A$). The solid line shows the predicted trend according to the differences listed in Table 12.

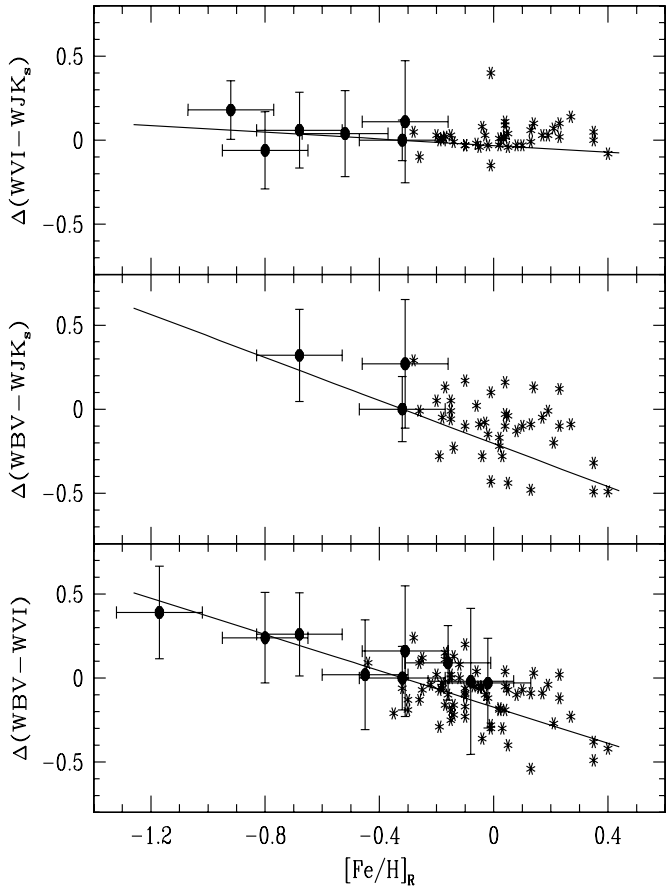

Figure 14. Same as in Figure 13, but with $[Fe/H]_R$ values by Romaniello and collaborators.

Table 13
Mean LMC-relative True Distance Moduli of External Galaxies Based on Cepheids with $0.5 \leqslant \log P \leqslant 2.0$ and the LMC *P–W* Relations Discussed in the Text

Galaxy	Met.	$\delta\mu_0(WBV)$	$\delta\mu_0(WVI)$	$\delta\mu_0(WJK_s)$
SextA	7.49	7.57 ± 0.19	7.18 ± 0.24	...
SextB	7.56	7.69 ± 0.51	...	...
WLM	7.74	...	6.58 ± 0.11	6.40 ± 0.18
IC1613[a]	7.86	6.17 ± 0.27	5.93 ± 0.13	...
IC1613[b]	7.86	...	5.72 ± 0.13	5.78 ± 0.22
SMC	7.98	0.73 ± 0.23	0.45 ± 0.12	0.41 ± 0.20
N6822	8.14	...	4.88 ± 0.22	4.84 ± 0.18
N0598o	8.21	6.17 ± 0.31	6.15 ± 0.19	...
N0300	8.35	8.14 ± 0.32	7.98 ± 0.29	7.87 ± 0.28
N4258o	8.50	10.99 ± 0.21	10.90 ± 0.13	...
N0598i	8.58	5.89 ± 0.30	5.91 ± 0.27	...
N4258i	8.64	10.65 ± 0.21	10.68 ± 0.21	...
N0224	8.68	5.66 ± 0.25	...	...
N0055	...	...	8.02 ± 0.38	7.91 ± 0.28
N0247	...	...	9.35 ± 0.35	9.18 ± 0.20

Notes. The galaxies are ordered by metal abundance.
[a] Antonello et al. (2006).
[b] Udalski et al. (2001), Pietrzynski et al. (2006a).

dex^{-1} which is in fair agreement with the value -0.5 mag dex^{-1} inferred from the predicted differences listed in Table 12.

To provide an independent test and to include in the current analysis more metal-rich Cepheids, we applied the above procedure to the Galactic Cepheids with measured iron-to-hydrogen ratios, without the need to know their distance. The source of the $BVIJK_s$ magnitudes was already mentioned in Section 2 and, to overcome possible systematic uncertainties in abundance measurements, we adopted the two largest sets of Cepheid metallicities available in the literature: the iron abundances $[Fe/H]_A$ provided by Andrievsky and collaborators (Andrievsky et al. 2002a, 2002b, 2002c; Andrievsky et al. 2004; Luck et al. 2003; Kovtyukh et al. 2005; Luck et al. 2006) and the iron abundances $[Fe/H]_R$ by Romaniello et al. (2005, 2008) and Lemasle et al. (2007, 2008). We selected the Galactic variables with $\log P > 0.5$, although the inclusion of first overtone pulsators has no significant impact upon the *differences* among the $\delta\mu_0(W)$ values.

Eventually, Figures 13 and 14 show that extragalactic and Galactic Cepheids follow well-defined common relations which are fully consistent with the predicted behaviors presented in Table 12, and further confirm that the metallicity effect on the *P–W* relations significantly depends on the adopted Wesenheit function.

As a consequence, if the LMC-based *P–W* relations are used to estimate the distance to Cepheids with metal content significantly different from the LMC abundance, then the values of the different relative distances $\delta\mu_0(W)$ should not be averaged, but taken into account individually, to further exploit the information provided by their different metallicity dependence.

5. METALLICITY CORRECTION(S) TO THE CEPHEID DISTANCE

A straightforward estimate of the metallicity effect on the Cepheid distance scale can be determined by using regions of the same galaxy located at different galactocentric distances and characterized by significantly different metal abundances. After the pioneering work by Freedman & Madore (1990) in M31, such a differential test was performed in NGC 5457 (Kennicutt et al. 1998, $\gamma = -0.24 \pm 0.16$ mag dex^{-1}), in NGC 4258 (Macri et al. 2006, $\gamma = -0.29 \pm 0.11$ mag dex^{-1}), and in NGC 598 (Scowcroft et al. 2009, hereinafter Sc09, $\gamma = -0.29 \pm 0.11$ mag dex^{-1}) giving an average value of $\gamma = -0.27$ mag dex^{-1}.

However, it is worth mentioning that the metallicity gradient in NGC 598, as already discussed by Sc09, is still a matter of debate and the use of the abundances of H II regions provided by Crockett et al. (2006) would provide a metallicity coefficient that is one order of magnitude larger ($\gamma = -2.90$ mag dex^{-1}). Moreover, the above results rely on the old metallicity scale provided by ZKH, and the use of the new metal abundances would imply significantly larger values of the metallicity coefficient γ with dramatic effects on the Cepheid distance scale. Moreover, Macri et al. (2001) showed that Cepheids in the inner field of NGC 5457 are severely affected by blending, which gives artificially shorter distances (Macri et al. 2006). Finally, we mention that van Leeuwen et al. (2007), using a *P–WVI* relation based on Galactic Cepheids and Cepheids in the inner field of NGC 4258, found a true distance (29.22 ± 0.03 mag) that agrees quite well with the maser distance (Herrnstein et al. 1999, 29.29 ± 0.15 mag). However, Mager et al. (2008) using Cepheids in the inner and in the outer field of NGC 4258 suggested that the difference in the true distance modulus of the two fields (29.26 ± 0.03 versus 29.45 ± 0.08 mag) might be due either to a difference in the reddening law or to small number statistics (see also Di Benedetto 2008). On these grounds, the quoted available differential tests in external galaxies need to be treated cautiously.

Robust constraints on the dependence of Cepheid distances on metallicity can also be provided by the comparison with distances based on an independent distance indicator. The tip of the red giant branch (TRGB) appears to be a robust standard candle, largely independent of metallicity in the *I* band (Madore et al. 2009; Sanna et al. 2008). However, we note that TRGB distances to galaxies characterized by complex star formation histories and age–metallicity relations might also be biased ($\Delta\mu \leqslant 0.10$ mag) due to the presence of TRGB stars younger than typical globular cluster counterparts (Salaris & Girardi 2005). In the following, we shall refer to the TRGB distances given by Rizzi et al. (2007, hereinafter Ri07) and listed in Column 2 of Table 14.

In the previous section, we showed that the pulsation models predict a rather strong metallicity effect on the distance modulus determined by using the *P–WBV* relation, whereas the distances based on the *P–WVI* and *P–WJK$_s$* relations appear rather independent of the Cepheid metal content. Data plotted in Figure 15 clearly show that such a prediction is fully consistent with the observations, and indeed, the comparison between the measured $\delta\mu_0(WBV)$ and $\delta\mu_0(WJK_s)$ listed in Table 13 with the TRGB distances yields metallicity coefficients γ that depend on the adopted passband. In particular, the TRGB distances provided by Ri07 give -0.52 ± 0.09 mag dex^{-1} and -0.05 ± 0.06 mag dex^{-1}, respectively. We note that these metallicity corrections agree quite well with the predicted values.

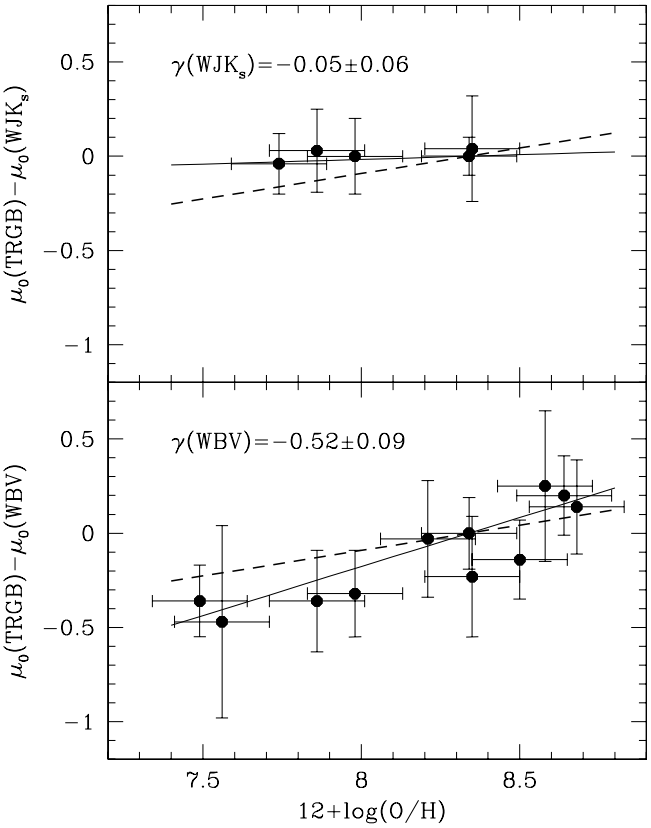

Figure 15. Difference between TRGB and Cepheid distances based on the *P–WBV* and on the *P–WJK$_s$* relation as a function of the nebular oxygen abundance. The solid line is the least-square fit to the data, while the dashed line is the average empirical value of the metallicity coefficient $\gamma = -0.277$ mag dex^{-1}.

Table 14
TRGB Distance Moduli Provided by Rizzi et al. (2007, Ri07)

Galaxy	Ri07
SextA	25.79 ± 0.06
SextB	25.79 ± 0.04
WLM	24.93 ± 0.04
IC1613	24.37 ± 0.05
SMC	18.98
N3109	25.56 ± 0.05
IC4182	28.23 ± 0.05
N0598	24.71 ± 0.04
N5457	29.34 ± 0.09
LMC	18.57
N0300	26.48 ± 0.04
N3031	27.69 ± 0.04
N3621	29.26 ± 0.12
N4258	29.42 ± 0.06
N0224	24.37 ± 0.10
N3351	29.92 ± 0.05
N5128	27.72 ± 0.04

Note. The galaxies are ordered by metal abundance.

The previously published Cepheid distances based on the *P–WVI* relation are summarized in Table 15. For the galaxies included in Table 8, the Cepheid sample is listed in Column 2, while Column 3 gives the distance modulus published in the original paper, but scaled to a homogeneous LMC distance modulus of $\mu_0 = 18.50$ mag. The galaxy distances provided by Freedman et al. (2001, hereinafter Fr01) are listed in Column 4. These distances were determined by using the LMC linear *P–L*

Table 15
Distance Moduli $\mu_0(WVI)$ for the Galaxies Listed in Table 8

Galaxy	Ref.[$\mu_{0,LMC}$]	Source	Fr01	Ka03	STT06	Our
IC1613[a]		...	24.19 ± 0.15	...	...	...
IC1613	(1)[18.50]	24.17 ± 0.07	...	...	...	24.22 ± 0.10
IC4182	Ka03	...	...	28.33 ± 0.13	...	28.35 ± 0.23
IC4182	KPr	...	28.28±0.06	...	...	28.25 ± 0.18
IC4182	STT06	...	...	...	28.28 ± 0.10	28.29 ± 0.18
LMC	STR04	18.50	18.50	18.50	18.50	18.50
N0055	(3)[18.50]	26.40 ± 0.05	...	...	...	26.47 ± 0.18
N0224	MF05	...	24.38 ± 0.05	...	24.35	...
N0247	(5,6)[18.50]	27.80 ± 0.09	...	...	...	27.84 ± 0.18
N0300	(8,9)[18.50]	26.43 ± 0.06	26.53 ± 0.07	...	26.44	26.44 ± 0.16

Notes. The number in square brackets in Column 2 is the LMC distance modulus adopted in the original paper.
[a] Data from Freedman (1988).
[b] Data from Freedman et al. (1991).
[c] Distance modulus from Sandage & Tammann (2008).

(This table is available in its entirety in a machine-readable form in the online journal. A portion is shown here for guidance regarding its form and content.)

relations from Udalski et al. (1999a) and $\mu_0(\mathrm{LMC}) = 18.50$ mag. In Column 5, we list the galaxy distances provided by Kanbur et al. (2003, hereinafter Ka03) using slightly revised LMC linear *P–L* relations of the same data given by Udalski et al. (1999a) and $\mu_0(\mathrm{LMC}) = 18.50$ mag. Column 6 gives the distance moduli determined by STT06 using LMC *P–L* relations with a break in the slope at $P = 10$ days. Since STT06 adopt $\mu_0(\mathrm{LMC}) = 18.54$ mag, the original values were scaled to a distance modulus of 18.50 mag.

A quick inspection of these data indicates that *on average* they are consistent with each other. However, for some individual galaxies, the difference among the various distances becomes of the order of ±0.2–0.3 mag. Since this discrepancy might be the consequence of different assumptions and procedures used to derive distances, we decided to provide new homogeneous estimates of the $\mu_0(WVI)$ distance moduli for the entire sample. The individual distances are listed in Column 6 by adopting the LMC relation of Equation (5) together with $\mu_0(\mathrm{LMC}) = 18.50$ mag and by applying a 2σ clipping.

We find that our distances are fully consistent with the values in the literature. The average difference between the new estimates and the distances listed in Columns 3–6 are the following: -0.01 ± 0.05 mag, $+0.02 \pm 0.06$ mag, $+0.03 \pm 0.05$ mag, and $+0.02 \pm 0.07$ mag, respectively. However, even though we used the same procedure, individual galaxy distance moduli might show a difference of the order of ∼0.2–0.3 mag, according to the various Cepheid samples.

By taking into account the entire sample, we show in Figure 16 the comparison between galactic Cepheid distances based on the the *P–WVI* relation and TRGB distances from Ri07. Once again, we found that the difference between Cepheid and TRGB distances gives a vanishing metallicity correction $-\gamma(WVI) = -0.03 \pm 0.07$ mag dex^{-1}—that agrees quite well with the predicted trend.

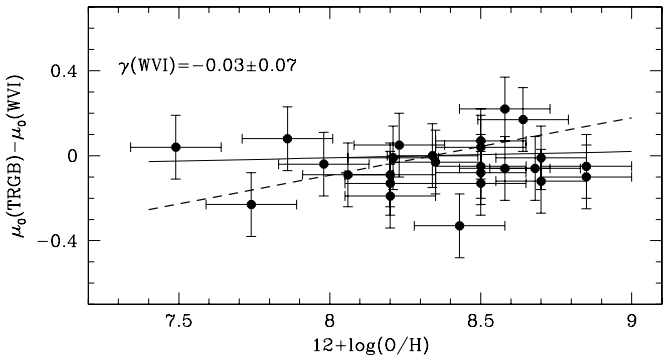

Figure 16. Differences between TRGB and Cepheid distances based on the *P–WVI* relation, as a function of the nebular oxygen abundance. The dashed line shows the average empirical value of the metallicity coefficient $\gamma = -0.27$ mag dex^{-1}.

6. SUMMARY

We performed a comprehensive investigation of the Cepheid distance scale by taking into account both theory and observations. In particular, we addressed the intrinsic features of both optical and NIR *P–L* relation. Here are the results:

1. *Filter wavelength.* Theory and observations indicate that the slopes of the *P–L* relation become steeper when moving from optical to NIR bands.
2. *Nonlinearity.* The slopes of the observed optical *P–L* relations of Magellanic Cepheids are nonlinear. No firm conclusion was reached concerning the nonlinearity of the *P–L* relations based on Galactic and M31 Cepheids.
3. *Period range.* The slopes of NIR *P–L* relations are less sensitive to the period range covered by Cepheids than the slopes of optical *P–L* relation.
4. *Metal content.* The derivative $\partial b_{\mathrm{all}}/\partial \log(Z/X)$ of the predicted slopes covering the entire period range decreases by more than a factor of 2 when moving from the *V*- to the *J* band and by almost one order of magnitude when moving from the *V*- to the *K* band. Moreover, the observed slopes of Magellanic, Galactic, and M31 Cepheids agree quite well with predicted ones. In particular, they suggest a flattening of the slope when moving from metal-poor to metal-rich Cepheids. This finding is at odds with the steepening recently suggested by TSR08, by STR08 and by ST08.

In order to provide an empirical estimate of the dependence of the *P–L* relation on metal content, we also adopted Cepheids in external Galaxies. To avoid possible deceptive uncertainties in the adopted metallicity scale, we derived a new relation to transform the old nebular oxygen abundances given by Zaritsky et al. (1994) into the new metallicity scale provided by Sakai et al. (2004).

Moreover, we provided new homogeneous estimates of *V*- and *I*-band slope for 87 independent Cepheid data sets available in the literature and 57 of them include more than

20 Cepheids. They are hosted in 48 external galaxies and for 27 of them two or more independent data sets are available. Four galaxies with multiple data sets (NGC 598, NGC 3031, NGC 4258, NGC 5457) have Cepheids located in an inner and in an outer galactic field. The galaxies with more than 20 Cepheids cover a wide metallicity range (12+log(O/H) $\sim$ 7.7 [WLM], 12+log(O/H) $\sim$ 8.9 dex [NGC 3351, NGC 4548]) Note that the quoted range is approximately a factor of 5 larger than the metallicity range covered by SMC (12+log(O/H) $\sim$ 8) and Galactic (12+log(O/H) $\sim$ 8.6) Cepheids. By using Cepheid data sets larger than 20, we tested three hypotheses concerning the dependence of the *P–L* relation on metal content:

1. *Correlation between the slope of the P–$L_{V,I}$ relations and the metallicity.* The χ^2 test on *V*- and *I*-band slopes indicates that this hypothesis can be discarded at the 99% confidence level.
2. *No dependence of the P–$L_{V,I}$ relations on the metallicity.* The χ^2 test on *V*- and *I*-band slopes indicates that this hypothesis can be accepted, but only at the 62% and 67% confidence level.
3. *Pulsation models predict that the slope of the P–$L_{V,I}$ relations becomes shallower in the metal-rich regime and constant in the metal-poor regime.* The outcome of the χ^2 test on observed *V*- and *I*-band slopes is that the predicted trend can be accepted at the 62% and 92% confidence level.

The main result of the above analysis based on external galaxies with sizable Cepheid samples is that the observed slopes of the *P–L_I* relation show the same metallicity trend predicted by pulsation models, while the slopes of the *P–L_V* relation either follow theory or do not depend on metallicity.

Together with the *P–$L_{V,I}$* relations we also investigated the reddening independent *P–W* relations and the results are the following:

1. *Dependence of the slope of the P–W relations on metal content.* Empirical estimates indicate that the slopes of optical (*P–WBV*, *P–WVI*) and NIR (*P–WJK_s*) relations in metal-poor and in metal-rich galaxies agree quite well with the slope of LMC Cepheids. This finding supports previous results by Benedict et al. (2007), Pietrzynski et al. (2007), van Leeuwen et al. (2007), and by Riess et al. (2009). Moreover, it brings forward the evidence that the *P–W* relations provide accurate estimates of LMC-relative true distance moduli. However, the metallicity dependence of the zero point of the *P–W* relations, if present, has to be taken into account.
2. *Use of the P–W relations as a metallicity diagnostic.* Current predictions indicate that LMC-relative true distance moduli based on the *P–WBV* relation strongly depend on the metal content, whereas those based on the *P–WVI* and on the *P–WJK_s* relation minimally depend on metallicity. The difference between the quoted distances can provide estimates of individual Cepheid metallicities.

The above findings further support the evidence that distances based on different *P–W* relations should not be averaged, since the metallicity effect strongly depends on the adopted bands.

Furthermore, we adopted the true distance moduli based on the TRGB method (Ri07) to validate the predicted metallicity corrections of the Cepheid distance scale. We found that the metallicity correction, γ, obtained using the TRGB distances, agrees quite well with pulsation predictions, namely $\gamma(WBV) = -0.52 \pm 0.09$ mag dex^{-1}, $\gamma(WVI) = -0.03 \pm 0.07$ mag dex^{-1}, and $\gamma(WJK) = -0.05 \pm 0.06$ mag dex^{-1}.

7. FINAL REMARKS AND FUTURE PERSPECTIVES

The results of this investigation rely on Cepheid samples which will soon become the templates to estimate the distances to late-type and dwarf irregular galaxies in the Local Group ($d \leqslant 1$ Mpc) and in the Local Volume ($d \leqslant 10$ Mpc). However, there are a few key points that demand future attention.

1. NIR mean magnitudes are only available for a handful of systems. Cepheid distances based on the predicted *P−WVI* and *P* − *WJK_s* relations are minimally dependent on the metallicity. Therefore, the difference can provide firm constraints on the plausibility of the assumption of an universal reddening law. This gap will certainly be filled by the James Webb Space Telescope[5] (Rieke et al. 2005) and the next generation of Extremely Large Telescopes[6] (Gilmozzi & Spyromilio 2009).
2. *B*-band mean magnitudes are only available for a handful of systems. The difference between Cepheid distances based on the predicted *P−WBV* and on the *P−WVI*/*P* − *WJK_s* relations is a robust diagnostic to estimate the Cepheid metal content. The significant sensitivity in the *B* band of the Wide Field Planetary Camera 3[7] (Wong et al. 2010) on board the *Hubble Space Telescope* can play a relevant role in this context.
3. The quest for solid constraints on the precision of the Cepheid distance scale brought forward the need for an accurate and homogeneous metallicity scale for external galaxies. Current findings rely on two relevant assumptions. (1) Oxygen abundances based on emission and on absorption lines appear to be rather similar (Hill 2004; Kudritzki et al. 2008; Bresolin et al. 2009), but new quantitative constraints in external galaxies are requested. (2) The oxygen appears to be a good proxy of the iron content (STT06). But oxygen is an α-element and it is not clear whether this approximation is still valid over the entire metallicity range.
4. The pulsation models currently adopted to constrain the properties of Galactic and external Cepheids were constructed assuming scaled-solar heavy element abundances. However, we still lack firm theoretical constraints on the impact of α-element abundances on their properties.
5. We plan to apply a theoretical homogeneous approach in the calibration of TRGB distances, of secondary distance indicators, and, eventually, in the estimate of the Hubble constant.

It is a pleasure to thank L. Rizzi for useful information on distance determinations to external galaxies based on the TRGB method. We acknowledge the referee, Prof. M. Feast, for his pertinent comments and suggestions that helped us to improve the content and the readability of the manuscript. We are very grateful to C. Jordi and V. Scowcroft for sending us their M31 and NGC 598 Cepheid catalog in electronic form. We also acknowledge A.R. Walker for his suggestions and for a detailed reading of an early version of this manuscript.

Note added in proof. Note that the synthetic *P–L* relation recently computed by Marconi et al. (2010) assuming a metal-poor chemical composition ($Z = 0.004$, $Y = 0.24$) agrees quite well with predictions for more metal-rich pulsators, namely $Z = 0.001$, $Z = 0.004$ (see Figure 1).

[5] More details can be found at the following URL: http://www.stsci.edu/jwst/
[6] More details can be found at the following URLs: http://www.eso.org/projects/e-elt/ and http://www.tmt.org/
[7] More details can be found at the following URL: http://www.stsci.edu/hst/wfc3

REFERENCES

Antonello, E., Fossati, L., Fugazza, D., Mantegazza, L., & Gieren, W. 2006, A&A, 445, 901
Andrievsky, S. M., Bersier, D., & Kovtyukh, V. V. 2002a, A&A, 384, 140
Andrievsky, S. M., Kovtyukh, V. V., & Luck, R. E. 2002b, A&A, 381, 32
Andrievsky, S. M., Kovtyukh, V. V., & Luck, R. E. 2002c, A&A, 392, 491
Andrievsky, S. M., Luck, R. E., Martin, P., & Lépine, J. R. D. 2004, A&A, 413, 159
Asplund, M., Grevesse, N., Sauval, A. J., Allende Prieto, C., & Kiselman, D. 2004, A&A, 417, 751
Benedict, G. F., et al. 2007, AJ, 133, 1810
Berdnikov, L. N., Dambis, A. K., & Vozyakova, O. V. 2000, A&AS, 143, 211
Berdnikov, L. N., Vozyakova, O. V., & Dambis, A. K. 1996, Astron. Lett., 22, 334
Bertelli, G., Nasi, E., Girardi, L., & Marigo, P. 2009, A&A, 508, 355
Bono, G., Caputo, F., Castellani, V., & Marconi, M. 1999a, ApJ, 512, 711 [Paper II]
Bono, G., Caputo, F., Fiorentino, G., Marconi, M., & Musella, I. 2008, ApJ, 684, 102
Bono, G., Marconi, M., & Stellingwerf, R. F. 1999b, ApJS, 122, 167 [Paper I]
Bono, G., et al. 2000, ApJ, 543, 955
Bresolin, F., Gieren, W., Kudritzki, R.-P., Pietrzyński, G., Urbaneja, M. A., & Carraro, G. 2009, ApJ, 700, 309
Caldwell, J. A. R., & Coulson, I. M. 1984, South African Astron. Soc. Obs. Circ., 8, 1
Cardelli, J. A., Clayton, G. C., & Mathis, J. S. 1989, ApJ, 345, 245
Caputo, F. 2008, Memorie della Soc. Astron. Ital., 79, 453
Caputo, F., Marconi, M., & Musella, I. 2000, A&A, 354, 610
Castellani, V., & Degl'Innocenti, S. 1995, A&A, 298, 827
Castellani, V., Degl'Innocenti, S., Marconi, M., Prada Moroni, P. G., & Sestito, P. 2003, A&A, 404, 645
Castelli, F., Gratton, R. G., & Kurucz, R. L. 1997a, A&A, 318, 841
Castelli, F., Gratton, R. G., & Kurucz, R. L. 1997b, A&A, 324, 432
Chiosi, C., Wood, P. R., & Capitanio, N. 1993, ApJS, 86, 541
Crockett, N. R., Garnett, D. R., Massey, P., & Jacoby, G. 2006, ApJ, 637, 741
Di Benedetto, G. P. 2008, MNRAS, 390, 1762
Dolphin, A. E., et al. 2003, AJ, 125, 1261
Ferrarese, L., Mould, J. R., Stetson, P. B., Tonry, J. L., Blakeslee, J. P., & Ajhar, E. A. 2007, ApJ, 654, 186
Fiorentino, G., Caputo, F., Marconi, M., & Musella, I. 2002, ApJ, 576, 402
Fiorentino, G., Marconi, M., Musella, I., & Caputo, F. 2007, A&A, 476, 863
Fouqué, P., et al. 2007, A&A, 476, 73 [Fo07]
Freedman, W. L. 1988, ApJ, 326, 691
Freedman, W. L., & Madore, B. F. 1990, ApJ, 365, 186
Freedman, W. L., Wilson, C. D., & Madore, B. F. 1991, ApJ, 372, 455
Freedman, W. L., et al. 2001, ApJ, 553, 47
García-Varela, A., et al. 2008, AJ, 136, 1770
Gibson, B. K., & Stetson, P. B. 2001, ApJ, 547, L103
Gieren, W., et al. 2004, AJ, 128, 1167
Gieren, W., et al. 2005, ApJ, 628, 695
Gieren, W., et al. 2006, ApJ, 647, 1056
Gieren, W., et al. 2008a, ApJ, 672, 266
Gieren, W., et al. 2008b, ApJ, 683, 611
Gieren, W., et al. 2009, ApJ, 700, 1141
Gilmozzi, R., & Spyromilio, J. 2009, in Astrophysics and Space Science Proceedings, Science with the VLT in the ELT Era, ed. A. Moorwood (Netherlands: Springer), 217
Girardi, L., Bressan, A., Bertelli, G., & Chiosi, C. 2000, A&AS, 141, 371
Groenewegen, M. A. T. 2008, A&A, 488, 25 [Gr08]
Groenewegen, M. A. T., Romaniello, M., Primas, F., & Mottini, M. 2004, A&A, 420, 655
Herrnstein, J. R., et al. 1999, Nature, 400, 539
Hill, V. 2004, in Origin and Evolution of the Elements, ed. A. McWilliam & M. Rauch (Cambridge: Cambridge Univ. Press), 203
Kanbur, S. M., Ngeow, C., Nikolaev, S., Tanvir, N. R., & Hendry, M. A. 2003, A&A, 411, 361 [Ka03]
Kennicutt, R. C., Jr., Bresolin, F., & Garnett, D. R. 2003, PASP, 115, 928
Kennicutt, R. C., Jr., Stetson, P. B., & Saha, A. 1998, ApJ, 498, 181
Kovtyukh, V. V., Wallerstein, G., & Andrievsky, S. M. 2005, PASP, 117, 1173
Kudritzki, R.-P., Urbaneja, M. A., Bresolin, F., Przybilla, N., Gieren, W., & Pietrzynski, G. 2008, ApJ, 681, 269
Laney, C. D., & Caldwell, J. A. R. 2007, MNRAS, 377, 147
Laney, C. D., & Stobie, R. S. 1986, MNRAS, 222, 449
Lemasle, B., Francois, P., Bono, G., Mottini, M., Primas, F., & Romaniello, M. 2007, A&A, 467, 283
Lemasle, B., François, P., Piersimoni, A., Pedicelli, S., Bono, G., Laney, C. D., Primas, F., & Romaniello, M. 2008, A&A, 490, 613
Leonard, D. C., Kanbur, S. M., Ngeow, C.-C., & Tanvir, N. R. 2003, ApJ, 594, 247
Luck, R. E., Kovtyukh, V. V., & Andrievsky, S. M. 2006, AJ, 132, 902
Luck, R. E., et al. 2003, A&A, 401, 939
Macri, L. M., Stanek, K. Z., Bersier, D., Greenhill, L. J., & Reid, M. J. 2006, ApJ, 652, 1133
Macri, L. M., et al. 2001, ApJ, 549, 721
Madore, B. 1982, PASP, 94, 40
Madore, B., & Freedman, W. L. 1991, PASP, 103, 933
Madore, B., & Freedman, W. L. 2009, ApJ, 696, 1498
Madore, B. F., Freedman, W. L., Catanzarite, J., & Navarrete, M. 2009, ApJ, 694, 1237
Madore, B. F., Mager, V., & Freedman, W. L. 2009, ApJ, 690, 389
Mager, V. A., Madore, B. F., & Freedman, W. L. 2008, ApJ, 689, 721
Marconi, M. 2009, Memorie della Soc. Astron. Ital., 80, 141
Marconi, M., Musella, I., & Fiorentino, G. 2005, ApJ, 632, 590
Marconi, M., et al. 2010, ApJ, 713, 615
McCommas, L. P., Yoachim, P., Williams, B. F., Dalcanton, J. J., Davis, M. R., & Dolphin, A. E. 2009, AJ, 137, 4707 [McC09]
Newman, J. A., et al. 2001, ApJ, 553, 562
Ngeow, C.-C., & Kanbur, S. M. 2004, MNRAS, 349, 1130
Ngeow, C.-C., & Kanbur, S. M. 2005, MNRAS, 360, 1033
Ngeow, C.-C., & Kanbur, S. M. 2006, ApJ, 642, 29
Ngeow, C.-C., Kanbur, S. M., & Nanthakumar, A. 2008, A&A, 477, 621 [NKN08]
Ngeow, C.-C., Kanbur, S. M., Nikolaev, S., Buonaccorsi, J., Cook, K. H., & Welch, D. L. 2005, MNRAS, 363, 831
Persson, S. E., Madore, B. F., Krzeminski, W., Freedman, W. L., Roth, M., & Murphy, D. C. 2004, AJ, 128, 2239 [Pe04]
Pietrinferni, A., Cassisi, S., Salaris, M., & Castelli, F. 2004, ApJ, 612, 168
Pietrzynski, G., et al. 2004, AJ, 128, 2815
Pietrzynski, G., et al. 2006a, ApJ, 642, 216
Pietrzynski, G., et al. 2006b, AJ, 132, 2556
Pietrzynski, G., et al. 2006c, ApJ, 648, 366
Pietrzynski, G., et al. 2007, AJ, 134, 594
Piotto, G., Capaccioli, M., & Pellegrini, C. 1994, A&A, 287, 371
Rieke, M. J., Kelly, D., & Horner, S. 2005, Proc. SPIE, 5904, 1
Riess, G. A., et al. 2005, ApJ, 627, 579
Riess, G. A., et al. 2009, ApJS, 183, 109 [Ri09]
Rizzi, L., Tully, R. B., Makarov, D., Makarova, L., Dolphin, A. E., Sakai, S., & Shaya, E. J. 2007, ApJ, 661, 815 [R07]
Romaniello, M., et al. 2005, A&A, 429, 37
Romaniello, M., et al. 2008, A&A, 488, 731
Saha, A., Thim, F., Tammann, G. A., Reindl, B., & Sandage, A. 2006, ApJS, 165, 108 [STT06]
Sakai, S., Ferrarese, L., Kennicutt, R. C., Jr., & Saha, A. 2004, ApJ, 608, 42 [Sa04]
Salaris, M., & Girardi, L. 2005, MNRAS, 357, 669
Sandage, A., & Tammann, G. A. 2008, ApJ, 686, 779 [ST08]
Sandage, A., Tammann, G. A., & Reindl, B. 2004, A&A, 424, 43 [STR04]
Sandage, A., Tammann, G. A., & Reindl, B. 2009, A&A, 493, 471
Sanna, N., et al. 2008, ApJ, 688, L69
Sasselov, D. D., et al. 1997, A&A, 324, 471
Scowcroft, V., Bersier, D., Mould, J. R., & Wood, P. R. 2009, MNRAS, 396, 1287 [Sc09]
Soszynski, I., Gieren, W., Pietrzynski, G., Bresolin, F., Kudritzki, R.-P., & Storm, J. 2006, ApJ, 648, 375
Stetson, P. B., & Gibson, B. K. 2001, MNRAS, 328, L1
Storm, J., Carney, B. W., Gieren, W. P., Fouqué, P., Latham, D. W., & Fry, A. M. 2004, A&A, 415, 531 [S04]
Tammann, G. A., Sandage, A., & Reindl, B. 2003, A&A, 404, 423
Tammann, G. A., Sandage, A., & Reindl, B. 2008, ApJ, 679, 52 [TSR08]
Tanvir, N. R., Ferguson, H. C., & Shanks, T. 1999, MNRAS, 310, 175
Thim, F., et al. 2003, ApJ, 590, 256
Udalski, A., et al. 1999a, Acta Astron., 49, 223
Udalski, A., et al. 1999b, Acta Astron., 49, 437
Udalski, A., et al. 2001, Acta Astron., 51, 221
Valle, G., Marconi, M., Degl'Innocenti, S., & Prada Moroni, P. G. 2009, A&A, 507, 1541
van Leeuwen, F., Feast, M. W., Whitelock, P. A., & Laney, C. D. 2007, MNRAS, 379, 723
Vilardell, F., Jordi, C., & Ribas, I. 2007, A&A, 473, 847
Wong, M. H., et al. 2010, in Wide Field Camera 3 Instrument Handbook, Version 2.0, (Baltimore, MD: STScI)
Zaritsky, D., Kennicutt, R. C., Jr., & Huchra, J. 1994, ApJ, 420, 87